

Supporting Information

Hydrophobic Domain Flexibility enables Morphology Control of Amphiphilic Systems in Aqueous Media

Ingo Helmers,^[a] Nils Bäumer^[a] and Gustavo Fernández^{*[a]}

[a] Organisch-Chemisches-Institut
Westfälische-Wilhelms-Universität Münster
Correnstrasse 40, 48149 Münster (Germany)
E-mail: fernandg@uni-muenster.de

Table of Contents

<i>Experimental Procedures</i>	S3
<i>Materials and Methods</i>	S3
<i>Synthetic details and characterization</i>	S4-S9
<i>Results and Discussion</i>	S10-S30
<i>Nucleation-Elongation model</i>	S10
<i>Denaturation model</i>	S10
<i>Thermodynamic Parameters</i>	S11
<i>Critical packing parameter ratio and estimation of the hydrophobic volume</i>	S12
<i>Supplementary Figures</i>	S13-S30
<i>References</i>	S31

Experimental Procedures

Materials and Methods

Chemical and Reagents: All chemicals were purchased from Sigma-Aldrich (St. Louis, MO, USA), TCI Europe N.V. (Tokyo, JP) or Alfa Aesar (Ward Hill, MA, USA), with minimum analytical grade quality and used without further purification unless otherwise stated. Dichloromethane was pre-dried over CaCl_2 and then distilled over P_2O_5 under argon atmosphere. Silica gel was used for column chromatography unless otherwise indicated.

Column chromatography. Preparative column chromatography was conducted in self-packed glass columns of different sizes with silica gel (particle size: 40 – 60 μm , *Merck*). Dichloromethane and methanol were distilled before usage.

NMR spectroscopy: ^1H and ^{13}C NMR spectra were recorded at 298 K on Avance II 300 and Avance II 400 from Bruker for routine experiments using tetramethylsilane (TMS) as internal reference, and DD2 500 and DD2 600 from Agilent for characterization purposes. Multiplicities for proton signals are abbreviated as s, d, t, q and m for singlet, doublet, triplet, quadruplet and multiplet, respectively.

Mass spectrometry: ESI mass spectra were measured on a Bruker MicrOTOF system.

UV/Vis and fluorescence spectroscopy: UV/Vis absorption spectra were recorded on a Jasco V-770 or a Jasco V-750 spectrophotometers, both equipped with peltier cells and Julabo F250 water circulation units. Fluorescence spectra were recorded on a Jasco FP-8500 spectrofluorometer equipped with the same water circulation unit.

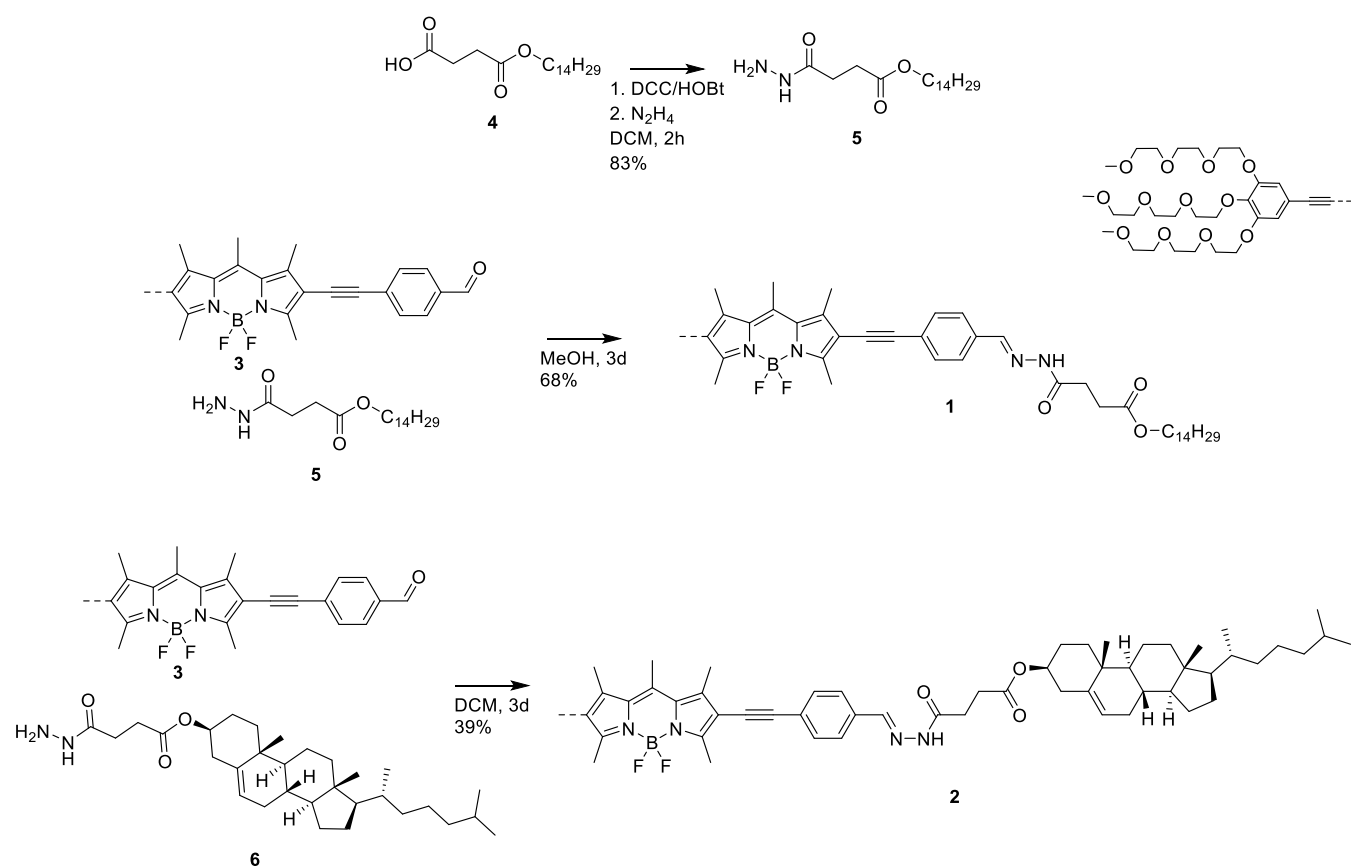
FT-IR spectroscopy: Solution and solid-state measurements were carried out using a JASCO-FT-IR-6800 and a CaF_2 cell with a path length of 0.1 mm. For all measurements, solvents of spectroscopic grade (UVasol) from Merck were used.

Dynamic and Static Light Scattering: DLS measurements were performed on a CGS-3 Compact Goniometer System from ALV, equipped with a LSE-5004 Light Scattering Electronics (22 mW HeNe Laser (633 nm)) and Multiple Tau Digital Correlator unit from ALV. Solvents were filtered prior to sample preparation through nylon or Teflon filters with a pore size of 0.45 μm .

AFM: The AFM images have been recorded on a *Multimode®8 SPM Systems* manufactured by *Bruker AXS*. The used cantilevers were *AC200TS* by *Oxford Instruments* with an average spring constant of 9 N m^{-1} , an average frequency of 150 kHz, an average length of 200 μm , an average width of 40 μm and an average tip radius of 7 nm. All solutions have been drop casted onto a mica surface using a volume of 10 μL .

Sample preparation method: Aggregates of **1** and **2** were dissolved in THF and subsequently diluted with the corresponding volume fraction of water to obtain the desired final concentration.

Synthetic Details and characterization

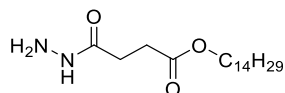


4-oxo-4-(tetradecyloxy)butanoic acid,¹ (3*S*,8*S*,9*S*,10*R*,13*R*,14*S*,17*R*)-10,13-dimethyl-17-((*R*)-6-methylheptan-2-yl)-2,3,4,7,8,9,10,11,12,13,14,15,16,17-tetradecahydro-1*H*-cyclopenta[*a*]phenanthren-3-yl 4-hydrazineyl-4-oxobutanoate² and 4-((5,5-difluoro-1,3,7,9,10-pentamethyl-8-((3,4,5-tris(2-(2-(2-methoxyethoxy)ethoxy)ethoxy)phenyl)ethynyl)-5*H*-5 λ^4 ,6 λ^4 -dipyrrolo[1,2-*c*:2',1'-*f*][1,3,2]diazaborin-2-yl)ethynyl)benzaldehyde³ were prepared following reported synthetic procedures and showed identical spectroscopic properties to those reported therein.

Synthesis of tetradecyl 4-hydrazineyl-4-oxobutanoate (5)

4-oxo-4-(tetradecyloxy)butanoic acid (**4**, 0.85 g, 2.72 mmol, 1 eq), DCC (0.56 g, 2.72 mmol, 1 eq) and HOBt (0.37 g, 2.72 mmol, 1 eq) were dissolved in DCM (30 mL) and stirred for 1 h at room temperature. The reactions were filtered and subsequently added to hydrazine hydrate (0.9 mL, 27.2 mmol, 10 eq). The reaction mixture was washed with a saturated Na₂CO₃ solution (3x 30mL). The organic phase was dried over MgSO₄ and the solvent was removed. Yield: 0.74 g (**5**, 2.26 mmol, 83%) of a white solid.

Characterization of **9**:



Chemical Formula: C₁₈H₃₆N₂O₃
 Exact Mass: 328,27
 Molecular Weight: 328,50

¹H NMR (500 MHz, CDCl₃): δ (in ppm) = 7.34 (s, 2H-N), 4.30 (s, 1H-N), 4.05 (t, J = 6.8 Hz, 2H-C-O), 2.66 (t, J = 6.9 Hz, 2H), 2.43 (t, J = 6.6 Hz, 2H), 1.59 (t, J = 6.8 Hz, 4H), 1.24 (d, J = 6.0 Hz, 20H), 0.86 (t, J = 7.0 Hz, 3H).

¹³C NMR (126 MHz, CDCl₃): δ (in ppm) = 173.0, 172.6, 65.2, 49.2, 34.0, 32.0, 29.8, 29.7, 29.6, 29.5, 29.4, 29.1, 28.7, 26.0, 25.7, 25.1, 22.8, 14.2.

ESI-MS (TOF): *m/z* 351.26155 [M+Na]⁺, calculated for C₁₈H₃₆N₂O₃Na: 351.26181

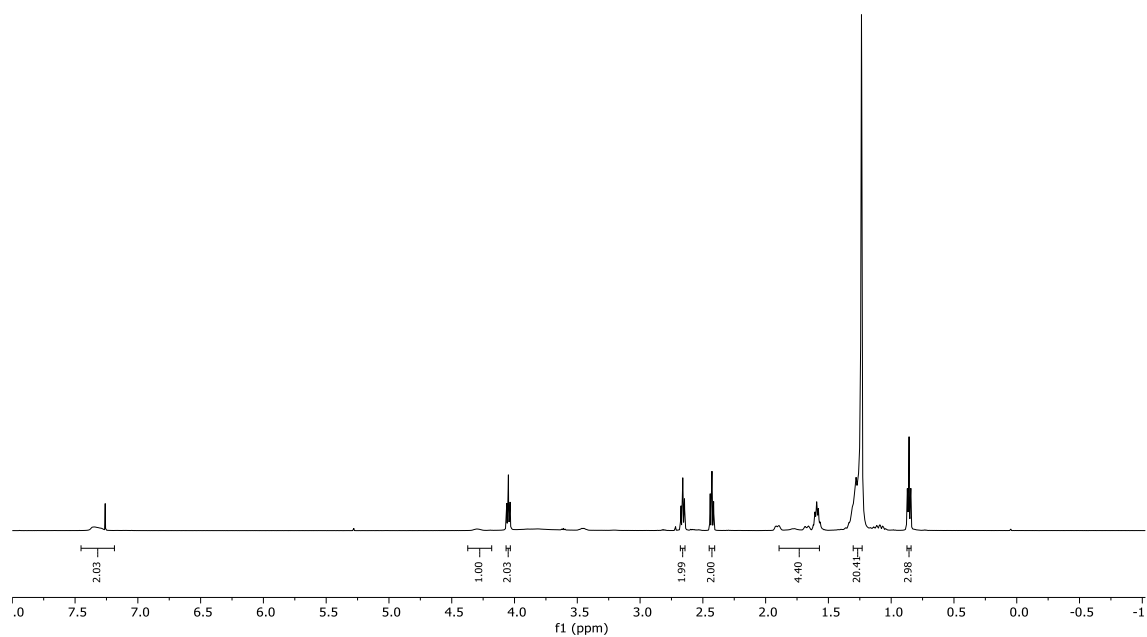


Figure S1. ^1H NMR (500 MHz, CDCl_3 , 298 K) of **5**.

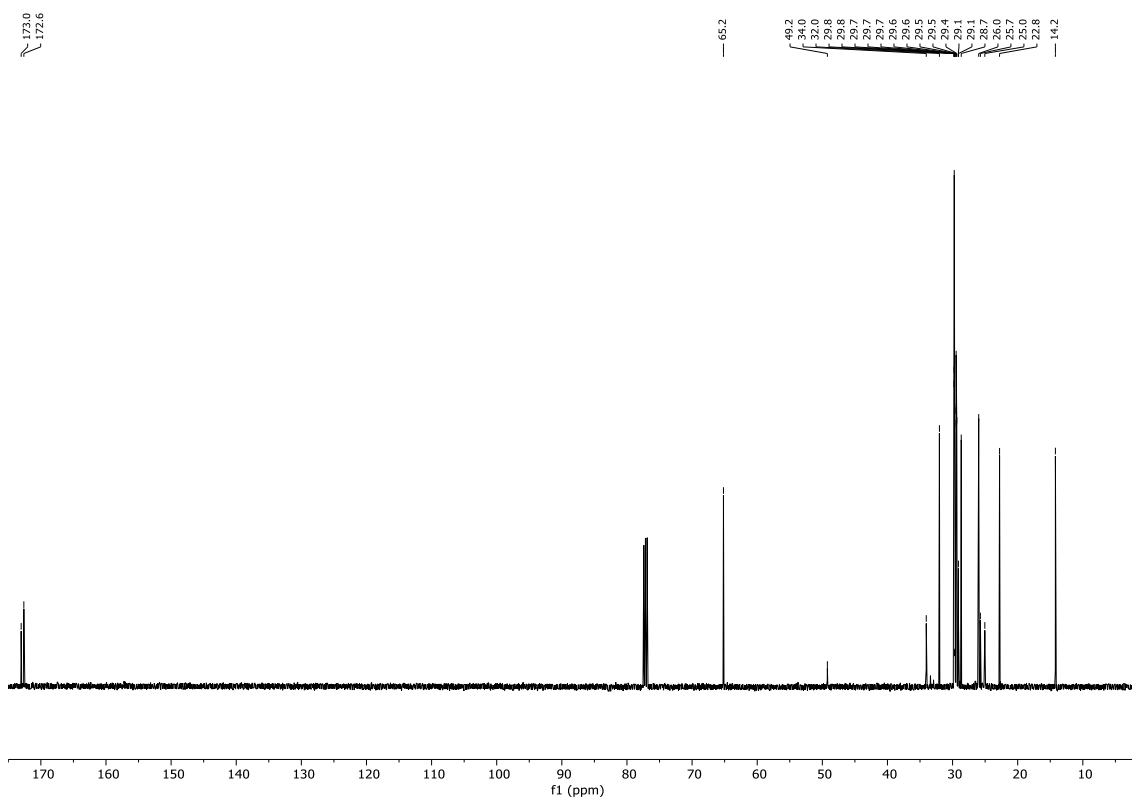


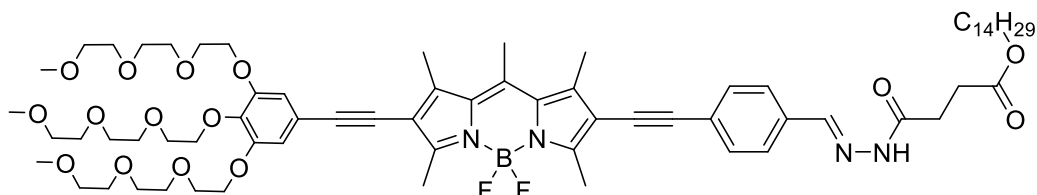
Figure S2. ^{13}C NMR (126 MHz, CDCl_3 , 298 K) of compound **5**.

tetradecyl

(*E*)-4-(2-(4-((5,5-difluoro-1,3,7,9,10-pentamethyl-8-((3,4,5-tris(2-(2-(2-methoxyethoxy)ethoxy)ethoxy)phenyl)ethynyl)-5*H*-5 λ^4 ,6 λ^4 -dipyrrolo[1,2-*c*:2',1'-*f*][1,3,2]diazaborinin-2-yl)ethynyl)benzylidene)hydrazineyl)-4-oxobutanoate (**1**)

4-((5,5-difluoro-1,3,7,9,10-pentamethyl-8-((3,4,5-tris(2-(2-(2-methoxyethoxy)ethoxy)ethoxy)phenyl)ethynyl)-5*H*-5 λ^4 ,6 λ^4 -dipyrrolo[1,2-*c*:2',1'-*f*][1,3,2]diazaborinin-2-yl)ethynyl)benzaldehyde (**3**, 30 mg, 0.031 mmol, 1 eq) and tetradecyl 4-hydrazineyl-4-oxobutanoate (**5**, 13.1 mg, 0.04 mmol, 1.3 eq) were dissolved in MeOH (10 mL), a drop of Trifluoroacetic acid was added and stirred for 3 days at room temperature. The mixture was concentrated and the crude product purified by silica gel column chromatography using a gradient from DCM (1/1, (v/v)) to DCM/MeOH (95/5, (v/v)) as eluent. Yield: 26.9 mg (**1**, 0.021 mmol, 68%) of a dark violet solid.

Characterization of **X**:



Chemical Formula: C₇₀H₁₀₁BF₂N₄O₁₅

Exact Mass: 1286,73

Molecular Weight: 1287,40

¹H NMR (600 MHz, CD₂Cl₂): δ (in ppm) = 8.87 (s, 1H-N), 7.74 (s, 1H-C=N), 7.66 (d, *J* = 8.4 Hz, 2H-Ar), 7.54 (d, *J* = 8.4 Hz, 2H-Ar), 6.80 (s, 2H-Ar-TEG), 4.21 (m, 6H-TEG), 4.07 (t, *J* = 6.7 Hz, 3H-C₁₄), 3.89 – 3.47 (m, 30H-TEG), 3.35 (m, 9H-TEG), 3.06 (t, *J* = 6.9 Hz, 2H), 2.74 – 2.53 (m, 17H-BODIPY(15H)), 1.67 – 1.56 (m, 4H-C₁₄), 1.26 (s, 20H-C₁₄), 0.88 (t, *J* = 7.0 Hz, 3H-C₁₄).

¹³C NMR (151 MHz, CD₂Cl₂): δ (in ppm) = 173.4, 172.7, 156.4, 152.2, 143.1, 142.1, 133.5, 131.4, 127.0, 125.0, 110.6, 98.6, 96.1, 87.0, 83.7, 72.2, 71.7, 71.5, 70.4, 70.3, 70.2, 70.1, 69.2, 68.5, 64.7, 58.7, 58.6, 31.9, 29.7, 29.6, 29.6, 29.5, 29.3, 28.6, 28.5, 27.8, 25.9, 22.6, 17.0, 16.0, 15.9, 13.8, 13.4.

ESI-MS (TOF): *m/z* 1287.74003 [M+H]⁺, calculated for C₇₀H₁₀₁N₄O₁₅BF₂ H: 1287.74087

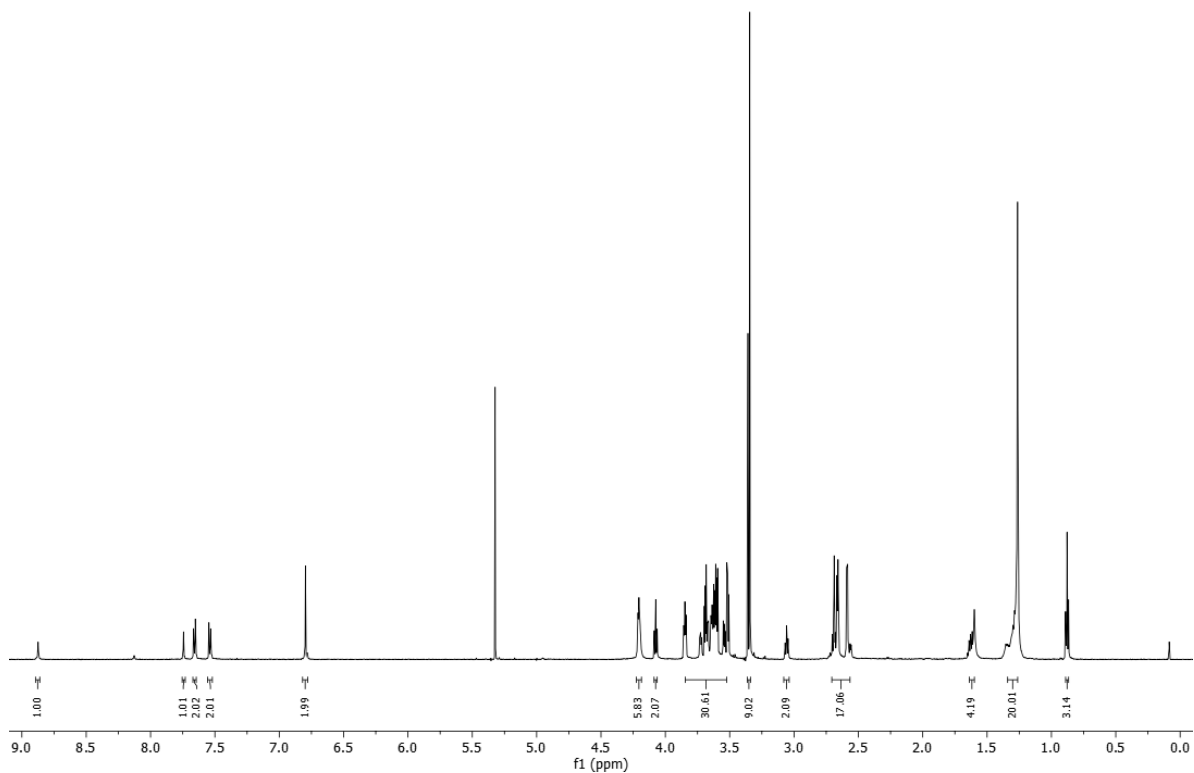


Figure S3. ^1H NMR (600 MHz, CD_2Cl_2 , 298 K) of **1**.

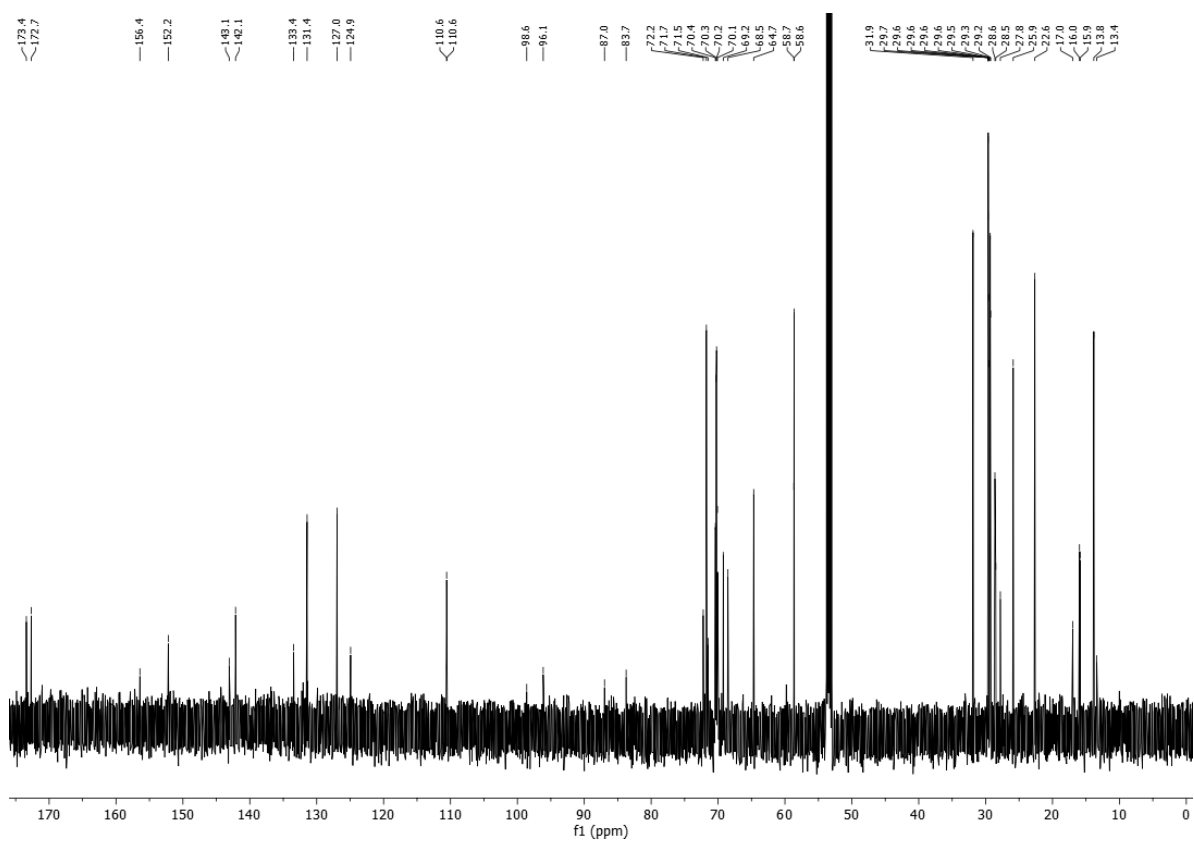


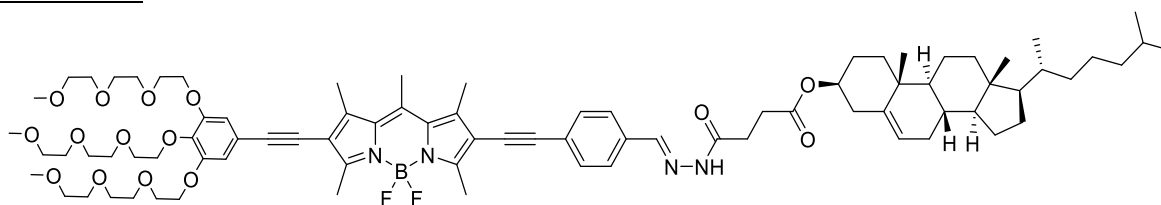
Figure S4. ^{13}C NMR (151 MHz, CD_2Cl_2 , 298 K) of **1**.

Synthesis of (3S,8S,9S,10R,13R,14S,17R)-10,13-dimethyl-17-((R)-6-methylheptan-2-yl)-2,3,4,7,8,9,10,11,12,13,14,15,16,17-tetradecahydro-1H-cyclopenta[a]phenanthren-3-yl 4-(2-((E)-4-((5,5-difluoro-1,3,7,9,10-pentamethyl-8-((3,4,5-tris(2-(2-(2-methoxyethoxy)ethoxy)ethoxy)phenyl)ethynyl)-5H-5 λ^4 ,6 λ^4 -dipyrrolo[1,2-c:2',1'-f][1,3,2]diazaborinin-2-yl)ethynyl)benzylidene)hydrazineyl)-4-oxobutanoate (2)

4-((5,5-difluoro-1,3,7,9,10-pentamethyl-8-((3,4,5-tris(2-(2-(2-methoxyethoxy)ethoxy)ethoxy)phenyl)ethynyl)-5H-5 λ^4 ,6 λ^4 -dipyrrolo[1,2-c:2',1'-f][1,3,2]diazaborinin-2-yl)ethynyl)benzaldehyde (**3**, 30.0 mg, 0.031 mmol, 1 eq) and (3S,8S,9S,10R,13R,14S,17R)-10,13-dimethyl-17-((R)-6-methylheptan-2-yl)-2,3,4,7,8,9,10,11,12,13,14,15,16,17-tetradecahydro-1H-cyclopenta[a]phenanthren-3-yl 4-hydrazineyl-4-oxobutanoate (**6**, 20.0 mg, 0.04 mmol, 1.3 eq) were dissolved in DCM (10 mL), a drop of Trifluoroacetic acid was added and stirred for 7 days at room temperature. The mixture was concentrated and the crude product purified by silica gel column chromatography using a gradient from DCM to DCM/MeOH (97/3, (v/v)) as eluent.

Yield: 17.7 mg (**2**, 0.012 mmol, 39%) of a dark violet solid.

Characterization of X:



Chemical Formula: C₈₃H₁₁₇BF₂N₄O₁₅

Exact Mass: 1458,86

Molecular Weight: 1459,67

¹H NMR (600 MHz, CD₂Cl₂): δ (in ppm) = 7.75 (s, 1H-C=N), 7.66 (d, J = 8.0 Hz, 2H-Ar), 7.53 (d, J = 7.9 Hz, 2H-Ar), 6.79 (s, 2H-Ar), 5.36 (d, J = 5.2 Hz, 1H-Chol), 4.62 – 4.55 (m, 1H-Chol), 4.23 – 4.17 (m, 6H-TEG), 3.86 – 3.48 (m, 30H-TEG), 3.35 (m, 9H-TEG), 3.05 (m, 2H), 2.71 – 2.56 (m, 15H-BODIPY), 2.32 (d, J = 8.0 Hz, 2H), 2.04 – 1.93 (m, 4H-Chol), 1.89 – 1.79 (m, 4H-Chol), 1.68 – 1.05 (m, 20H-Chol), 1.02 (s, 3H-Chol), 0.92 (d, J = 6.5 Hz, 3H-Chol), 0.86 (dd, J = 6.7, 2.4 Hz, 6H-Chol), 0.68 (s, 3H-Chol).

¹³C NMR (151 MHz, CD₂Cl₂): δ (in ppm) = 173.7, 172.1, 152.3, 143.1, 142.4, 139.8, 133.5, 131.4, 127.0, 124.9, 122.4, 110.6, 96.2, 83.8, 74.1, 72.3, 71.8, 71.6, 70.5, 70.4, 70.3, 70.2, 69.3, 68.6, 58.7, 58.6, 56.7, 56.2, 50.1, 42.2, 39.7, 39.4, 38.1, 37.0, 36.5, 36.1, 35.8, 31.9, 31.8, 29.7, 28.8, 28.2, 28.0, 27.8, 27.7, 24.2, 23.8, 22.5, 22.3, 21.0, 19.1, 18.5, 17.0, 16.0, 15.9, 13.4, 13.3, 11.6.

ESI-MS (TOF): m/z 1459.86599 [M+Na]⁺, calculated for C₈₃H₁₁₇N₄OBF₂H: 1459.86624

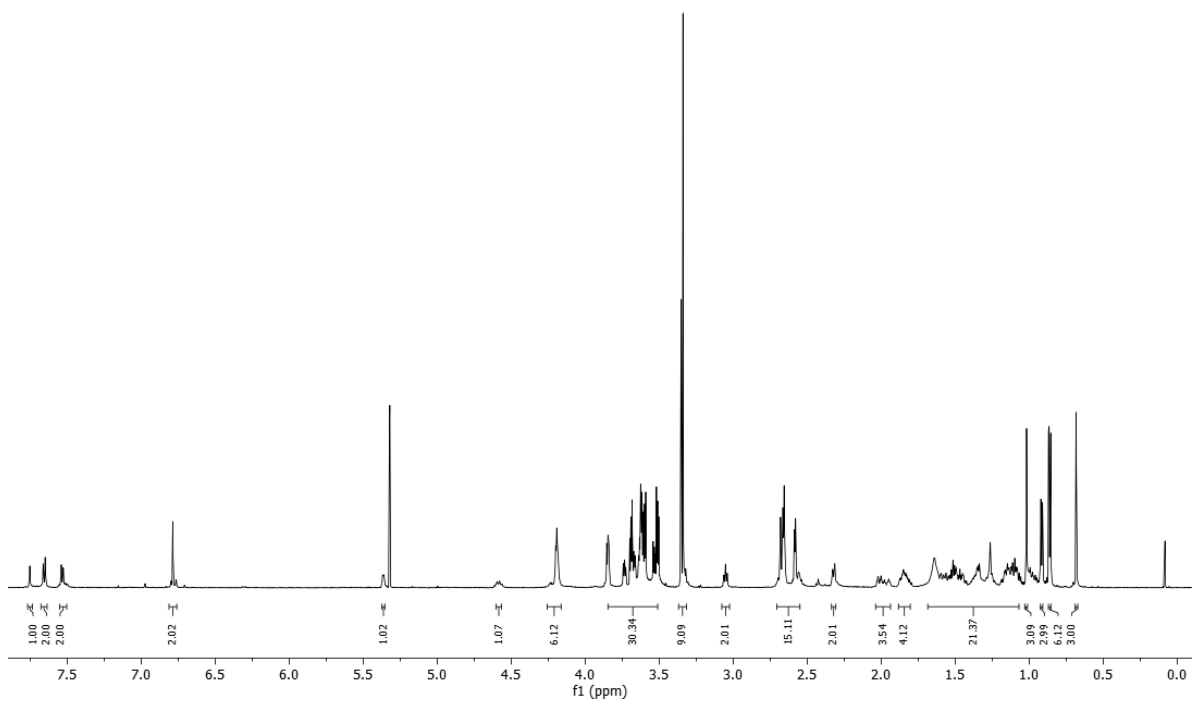


Figure S5. ^1H NMR (600 MHz, CD_2Cl_2 , 298 K) of **2**.

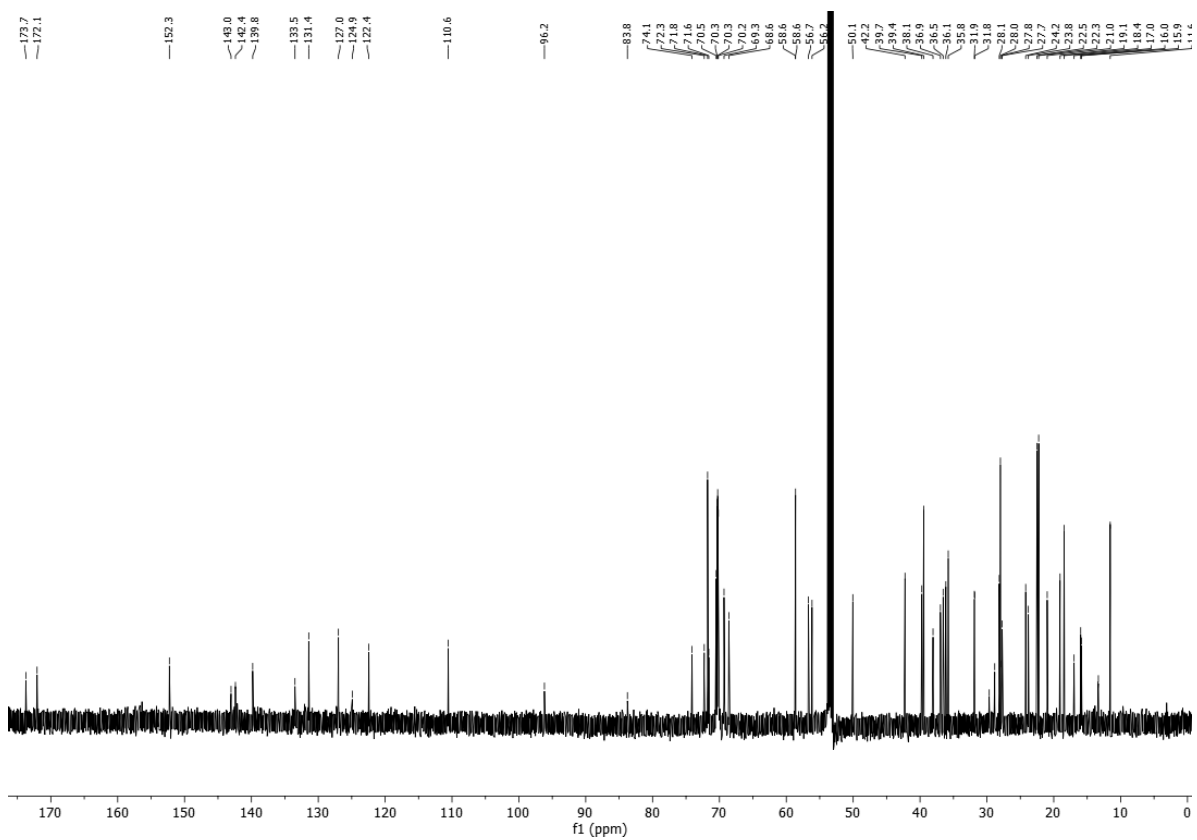


Figure S6. ^{13}C NMR (151 MHz, CD_2Cl_2 , 298 K) of compound **2**.

Results and Discussion

Nucleation-Elongation model for Cooperative Supramolecular Polymerizations

The equilibrium between the monomeric and supramolecular species can be described in a cooperative process with the *Nucleation-Elongation model* which is developed by Ten Eikelder, Markvoort and Meijer.^{4,5} This model is used to describe the aggregation of **1** and **2** which exhibit a non-sigmoidal cooling curve as shown in fluorescence and Uv-vis temperature-dependent experiments. The model extends nucleation-elongation based equilibrium models for growth of supramolecular homopolymers to the case of two monomer and aggregate types and can be applied to symmetric supramolecular copolymerizations, as well as to the more general case of nonsymmetric supramolecular copolymerizations.

In a cooperative process, the polymerization occurs by a nucleation step, to a nucleus size assumed of B, and a following elongation step. The values T_e , ΔH°_{nucl} , ΔH° and ΔS° can be determined by a non-linear least-square analysis of the experimental melting curves. The equilibrium constants associated with the nucleation and elongation phases can be calculated using equations **1** and **2**:

Nucleation step:

$$K_n = e^{\left(\frac{-(\Delta H^\circ - \Delta H^\circ_{nucl}) - T\Delta S^\circ}{RT}\right)} \quad (1)$$

Elongation step:

$$K = e^{\left(\frac{-(\Delta H^\circ - T\Delta S^\circ)}{RT}\right)} \quad (2)$$

And the cooperativity factor (σ) is given by:

$$\sigma = \frac{K_n}{K_e} = e^{\left(\frac{\Delta H^\circ_{nucl}}{RT}\right)} \quad (3)$$

Denaturation model⁶

The denaturation model is based on the concentration-dependent supramolecular polymerization equilibrium model by Goldstein,⁷ whereas the polymerization is described as a sequence of monomer addition equilibria.

$$[P_n] = K_n[P_{n-1}][X]$$

$$[P_{n+1}] = K_e[P_n][X]$$

$$[P_i] = K_e[P_{i-1}][X]$$

For cooperative model $K_n < K_e$ and for isodesmic process $K_n = K_e$. The concentration for each species P_i is given by $[P_i] = K_n^{i-1}[X]^i$ for $i \leq n$ and $[P_i] = K_e^{i-n}K_n^{n-1}[X]^i$ for $i > n$.

The dimensionless mass balance is obtained by inserting the dimensionless concentration

$p_i = K_e[P_i]$, monomer concentration $x = K_e[X]$ and concentration of each species

P_i (for $i \leq n$): $p_i = \sigma^{i-1}x^i$ and for $i > n$: $p_i = \sigma^{n-1}x^i$:

$$x_{tot} = \sigma^{-1} \sum_{i=1}^n i(\sigma x)^i + \sigma^{n-1} \sum_{i=n+1}^{\infty} ix^i.$$

Both sums are evaluated by using standard expressions for converging series:

$$x_{tot} = \left(\frac{(\sigma x)^{n+1}(n\sigma x - n - 1)}{(\sigma x - 1)^2} + \frac{\sigma x}{(\sigma x - 1)^2} \right) - \sigma^{n-1} \left(\frac{x^{n+1}(nx - n - 1)}{(x - 1)^2} \right)$$

With $x_{tot} = c_{tot}K_e$ and c_{tot} : the total monomer concentration

The sum solved by standard numerical methods (Matlabfzerosolver) results the dimensionless monomer concentration x .

Considering that every species with $i > 1$ is defined as aggregate, the degree of aggregation results in:

$$\varphi = \frac{x_{tot} - x}{x_{tot}}$$

Via $K_e = \exp(-\frac{\Delta G^0}{RT})$ the denaturation curves can be obtained with f defined as volume fraction of good solvent:

$$\Delta G^0 = \Delta G^0 + m f$$

It is assumed that the cooperativity factor σ is independent of the volume fraction and the m value involved in the elongation equals the m value involved in the nucleation.

The denaturation data need to be transformed into the normalized degree of aggregation, if fitted to the supramolecular polymerization equilibrium model:

$$(f) = \frac{A(f) - A(f = 0)}{A(f = 1) - A(f = 0)}$$

The optimization of the four needed parameters (ΔG_0 , m , σ and p) to fit the equilibrium model to the experimental data (normalized degree vs f) is done by the non-linear least-squares analysis using Matlab (lsqnonlinsolver). The data is then fitted with the non-linear least squared regression (Levenberg-Marquardt algorithm).

Thermodynamic Parameters

The thermodynamic parameters for **1** and **2** (Table S1-2) were obtained by fitting the respective experimental data to the denaturation model^[a] and globally ($c = 10, 15$ and $20 \mu\text{M}$) to the nucleation-elongation model^[b].

Table S1. Thermodynamic parameters of supramolecular polymerization of **1** and **2**.^[a]

$c / \mu\text{M}$	1	2
	$\Delta G_{298} / \text{kJ mol}^{-1}$	$\Delta G_{298} / \text{kJ mol}^{-1}$
10	-51.5	-57.0
20	-58.8	-60.9
40	-47.4	-54.1
\emptyset	-52.6	-57.3

Table S2. Thermodynamic parameters of supramolecular polymerization of **1** (THF/water (75/25)) and **2** (THF/water (65/35))^[b]

	$c / \mu\text{M}$	$\Delta H_0 / \text{kJ mol}^{-1}$	$\Delta S_0 / \text{kJ mol}^{-1} \text{T}^{-1}$	$\Delta H_{NP} / \text{kJ mol}^{-1}$	$\Delta G_{298} / \text{kJ mol}^{-1}$
1 UV	10-20	-134.15	-0.33	-11.82	-37.38
1 Emission	10-20	-93.86	-0.20	-13.02	-34.40
2 UV	10-20	-77.90	-0.15	-35.00	-34.34
2 Emission	10-20	-85.54	-0.17	-14.29	-34.10
2 CD	20	-85.73	-0.17	-13.15	-34.92

Critical packing parameter and estimation of the hydrophobic volume

The critical packing parameter is defined as:⁸

$$P_c = \frac{v}{a_0 \times l_c}$$

v : Volume of the hydrophobic group

a_0 : area of the hydrophilic group

l_c : hydrophobic group length

While l and a_0 is almost unaltered for the molecules **1** and **2**, the hydrophobic volume varies in their terminal group (tetradecan vs. cholesterol).

The volume of the alkane chains can be calculated with the following equation:⁸

$$v_1 = (27.4 + 26.9n) \times 10^{-3} \text{ nm}^3$$

n : number of carbon atoms

For a tetradecyl chain ($n = 14$), a volume of 0.404 nm^3 is observed.

The value for the cholesterol group can be estimated with help of:⁹

$$v_2 = \frac{m}{\rho}$$

m : mass of one cholesterol molecule ($\frac{386.67 \frac{\text{g}}{\text{mol}}}{6.022 \times 10^{23} \text{ mol}^{-1}}$)

ρ : density of cholesterol ($1.07 \frac{\text{g}}{\text{cm}^3}$)

The volume of cholesterol is observed as 0.687 nm^3

Since l_c and a_0 is the same in **1** and **2**. The relation between both packing parameters is:

$$\frac{P_{c(1)}}{P_{c(2)}} = \frac{v(1) \times a_{0(2)} \times l_{c(2)}}{v(2) \times a_{0(1)} \times l_{c(1)}} = \frac{v(1)}{v(2)} = \frac{0.404 \text{ nm}^3}{0.687 \text{ nm}^3} = 0.588$$

Typical values for different nanostructures are: micelles $0.33 > P_c$, cylindrical micelles $0.33 > P_c > 0.5$, flexible bilayers (vesicles) $0.5 > P_c > 1$, bilayers $P_c \sim 1$ and inverted micelles $1 > P_c$.

Since molecule **2** forms bilayer structures, the packing parameter is predicted to be $P_c \sim 1$. Based on this approximation, a value of 0.588 would be observed for **1**, which suggests the formation of vesicles. This does not agree with our experimental observation (formation of micelles).

Supplementary Figures

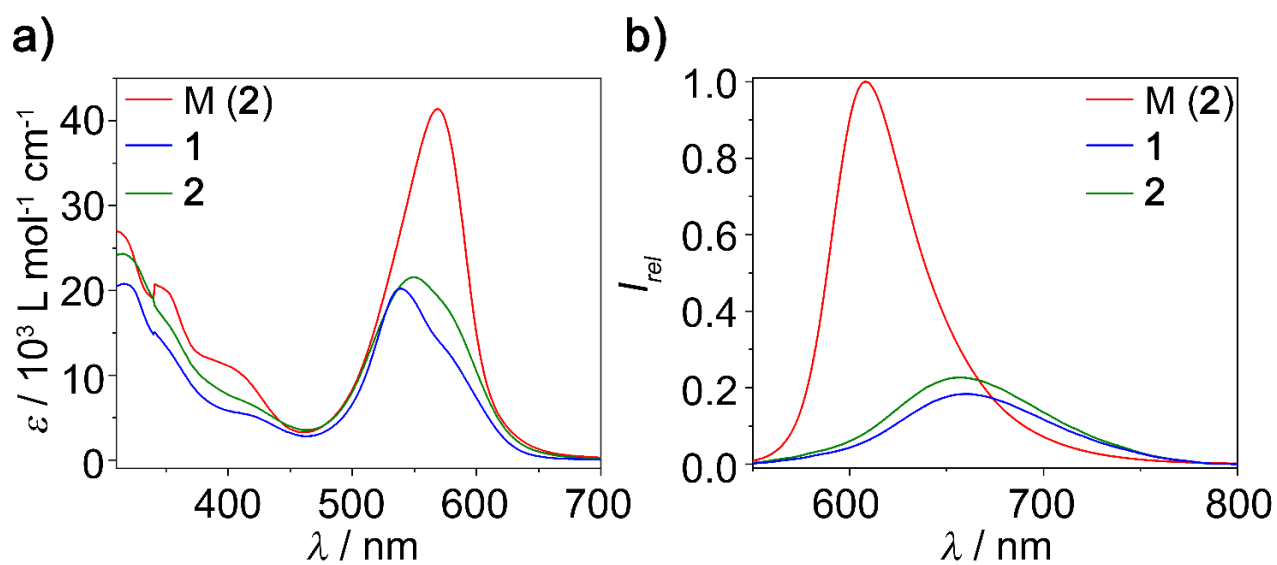


Figure S7. UV-Vis absorption (a) and emission spectra (b) of compound **1** and **2** in monomeric (only **2** shown due to minor changes in CHCl_3) and different aggregated states ($\text{H}_2\text{O}/\text{THF}$ (9/1) (v/v)), $c = 20 \mu\text{M}$ at 298 K. ($\lambda_{exc} = 530 \text{ nm}$ and Emission multiplied by 100 for aggregated state).

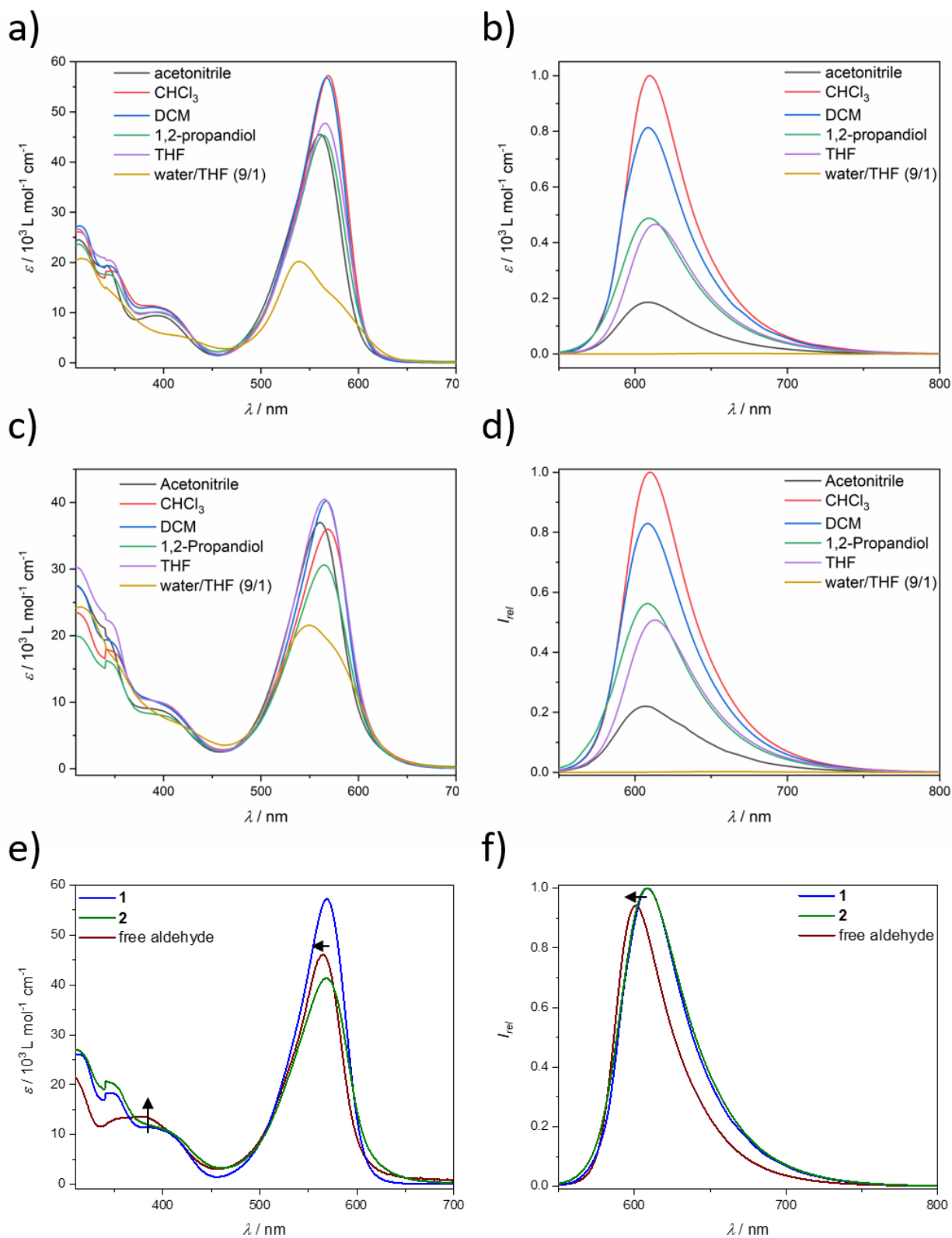


Figure S8. UV-Vis absorption (a, c, e) and emission spectra (b, d, f) of compounds **1** (top) and **2** (middle) in different solvents and comparison of monomeric spectra of **1**, **2** and free aldehyde (bottom) at 298 K and $c = 20 \mu\text{M}$. For emission spectra, an excitation wavelength of $\lambda = 530 \text{ nm}$ was applied.

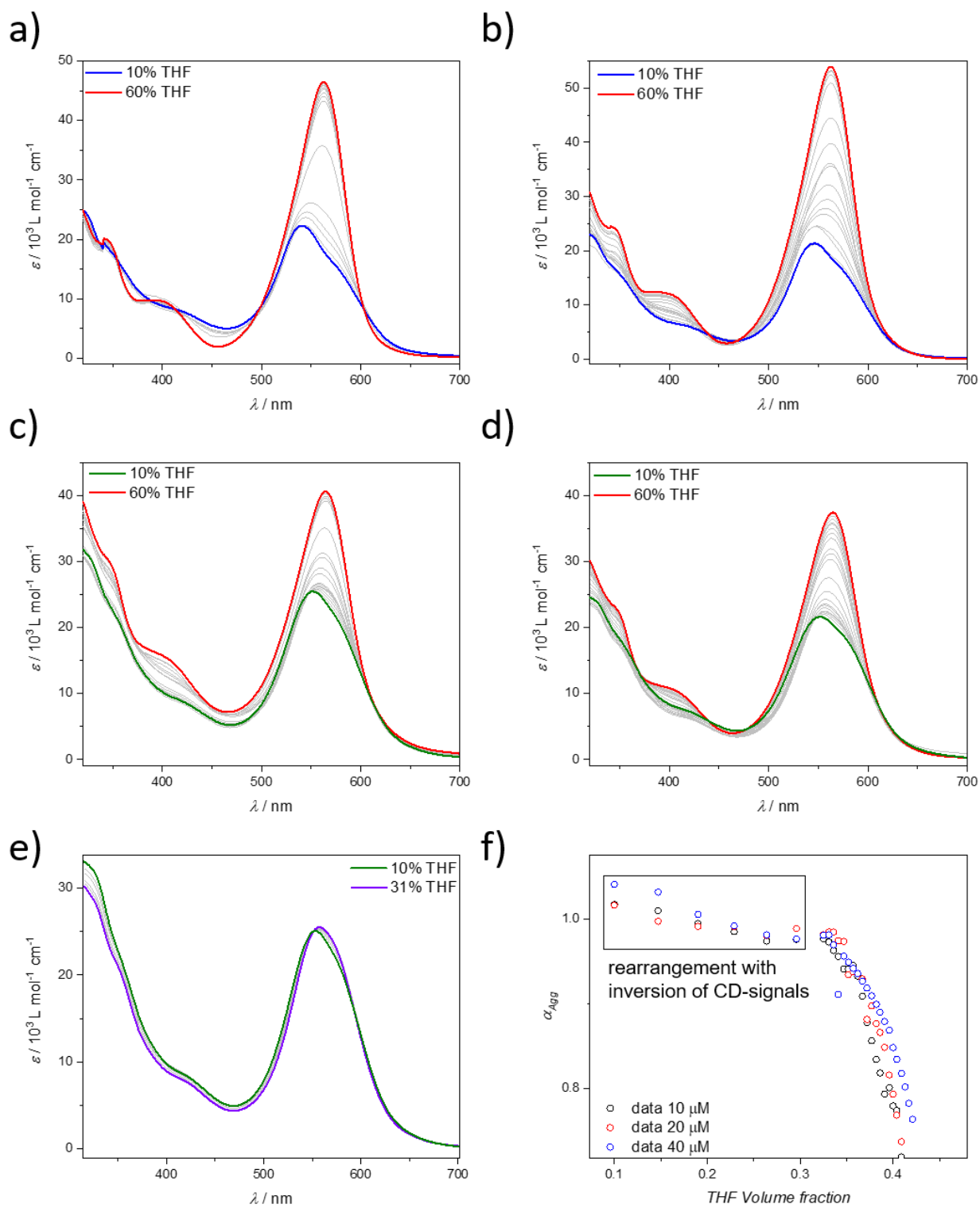


Figure S9. Denaturation UV-Vis Studies of **1** (10 μM (a) and 40 μM (b)) and **2** (10 μM (c) and 40 μM (d)) at 298 K. Spectra of **2** (e) at 20 μM and 298K and absorption changes (f) in the region of 10-31% THF Volume fraction.

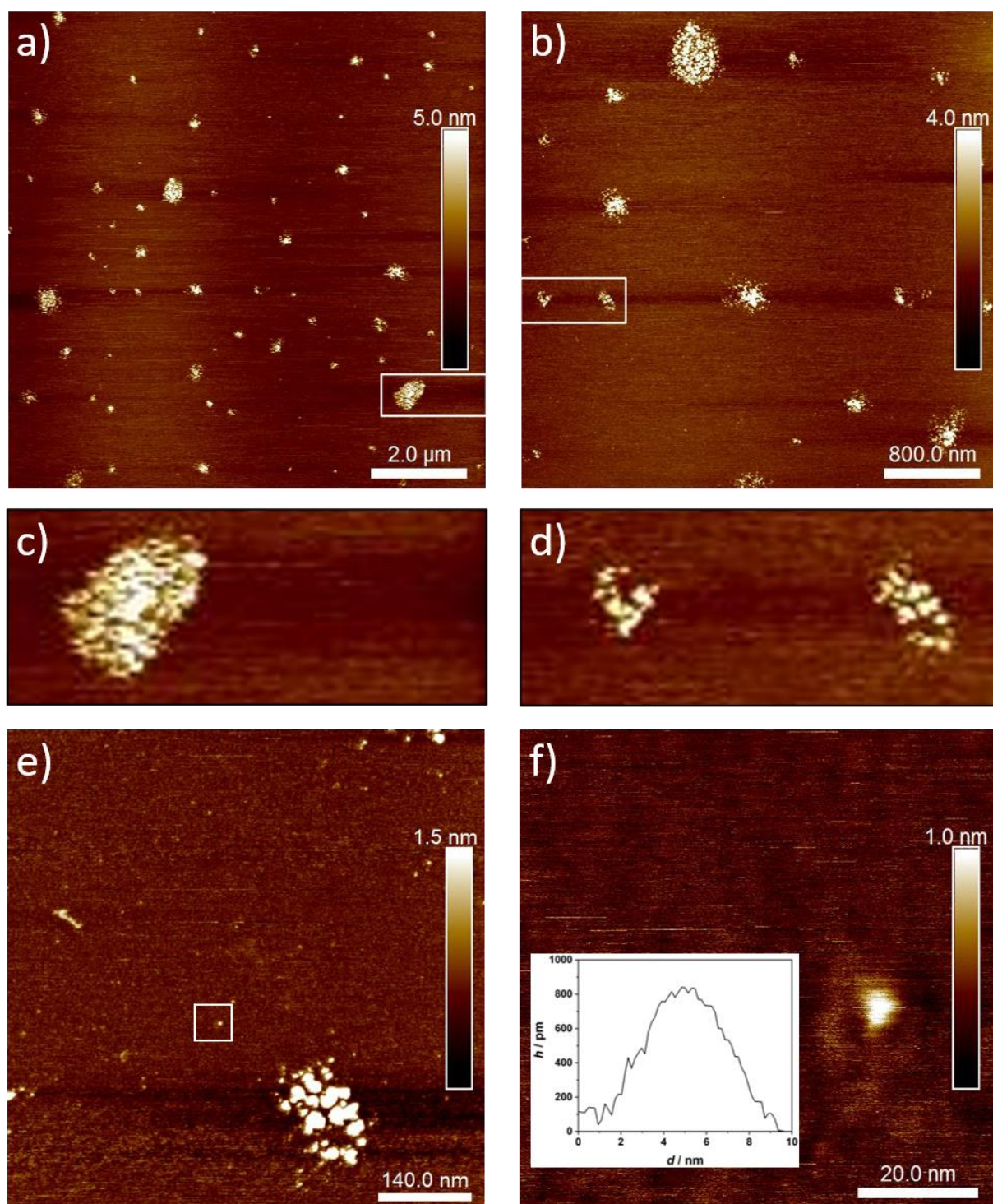


Figure S10. AFM images of **1** (a-f) in H₂O/THF (9/1 (v/v), $c = 2.0 \times 10^{-5}$ M) drop-casted onto a mica surface.

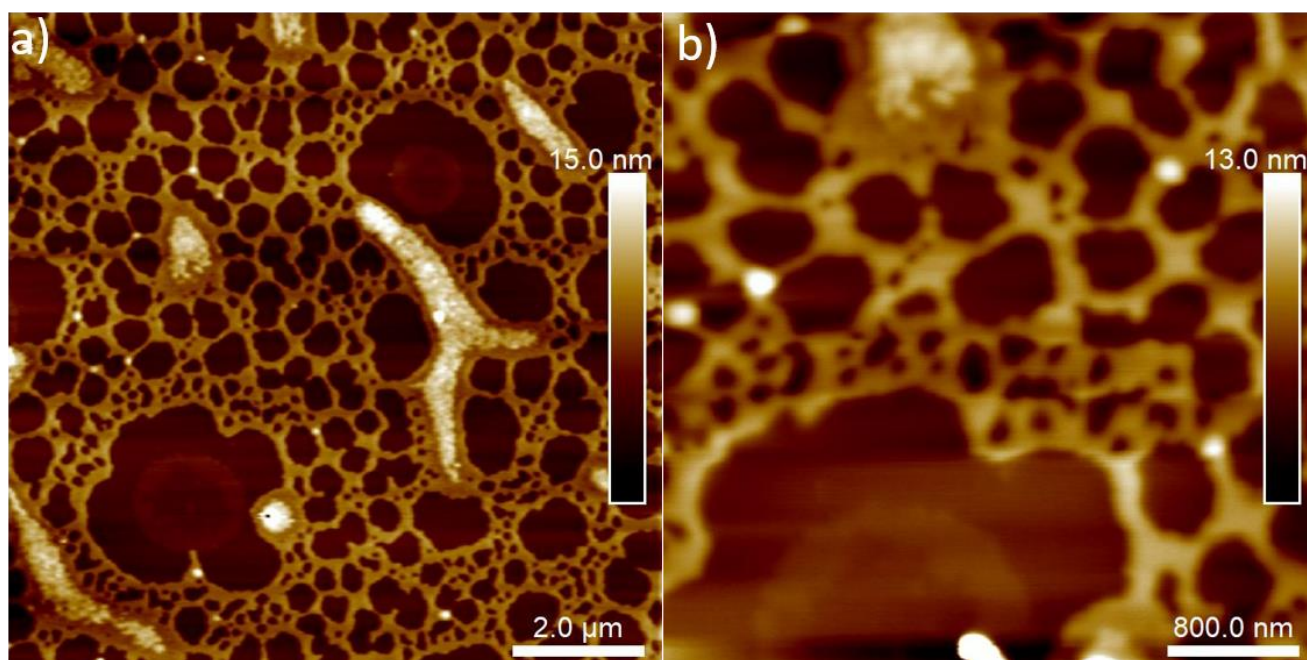


Figure S11. AFM images of **2A** (a-c) in H₂O/THF (9/1 (v/v), $c = 2.0 \times 10^{-5}$ M) drop-casted onto a mica surface.

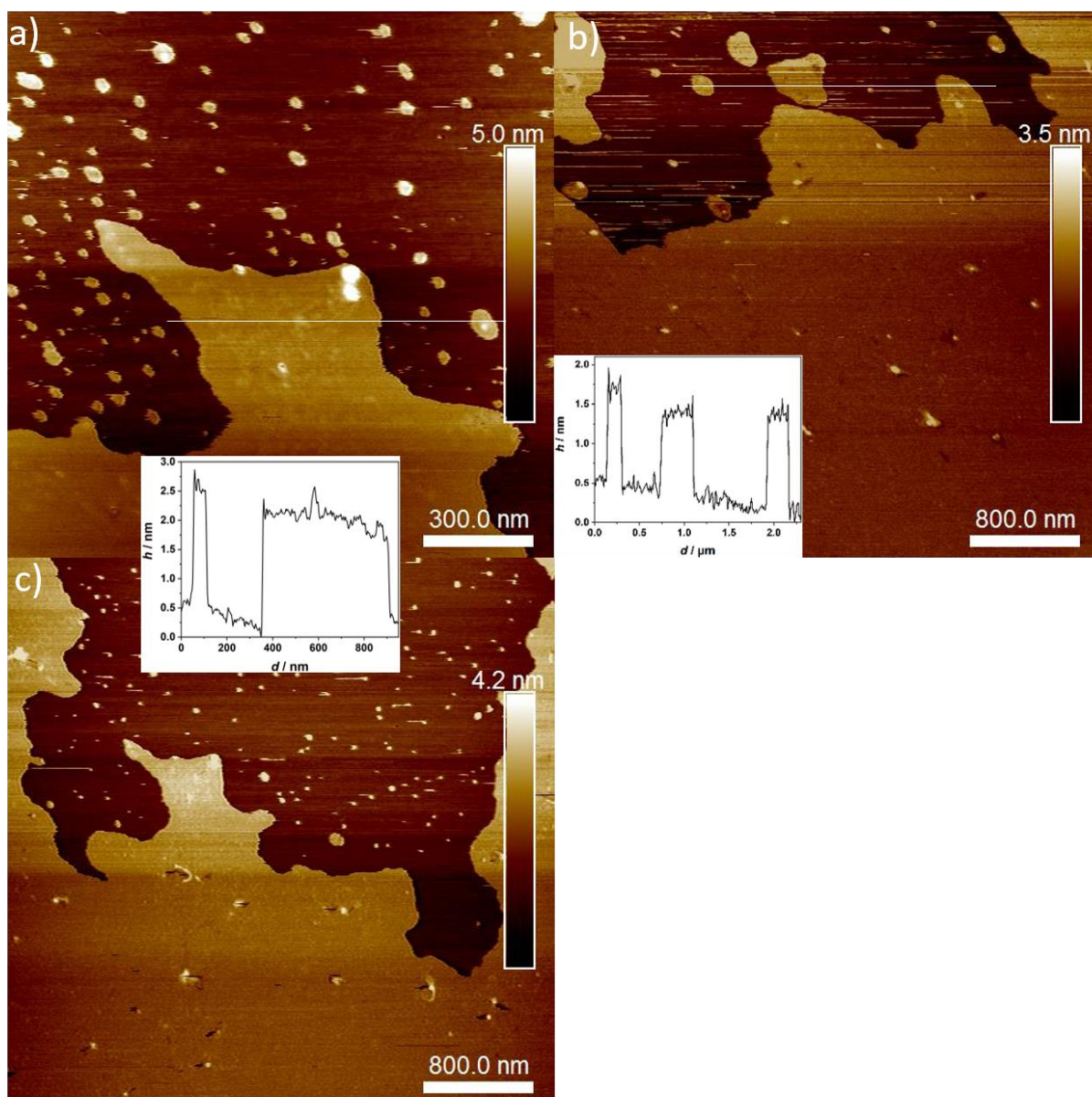


Figure S12. AFM images of **2B** (a-c) in $\text{H}_2\text{O}/\text{THF}$ (65/35 (v/v), $c = 2.0 \times 10^{-5} \text{ M}$) drop-casted onto a mica surface.

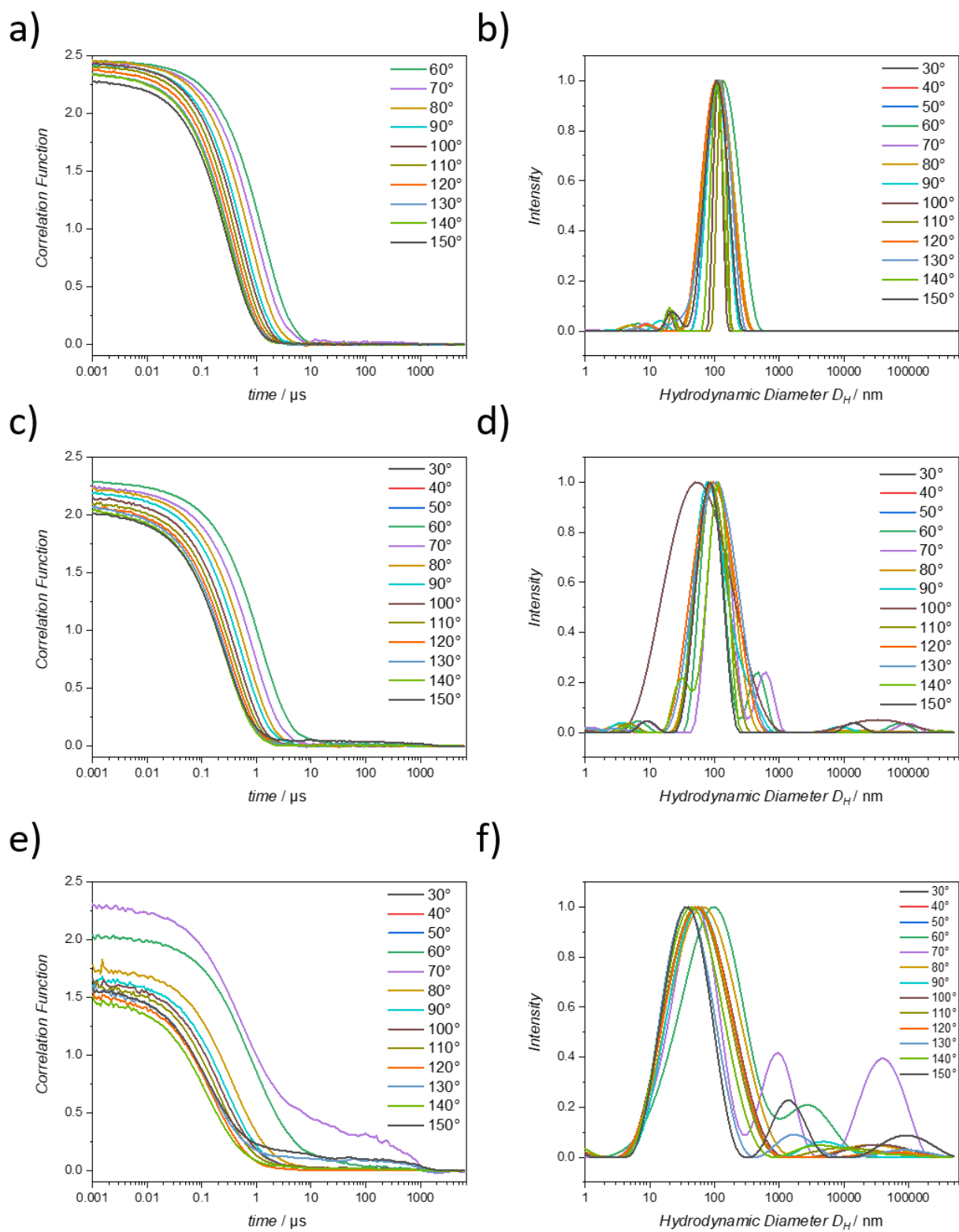


Figure S13. Angular dependent DLS studies. Size distribution and corresponding correlation function for **1** (a,b), **2A** (c,d) and **2B** (e,f). All studies have been performed at 298 K with the corresponding aggregate solutions (20 μM , 10% (**1** and **2A**) or 35% THF (**2B**)).

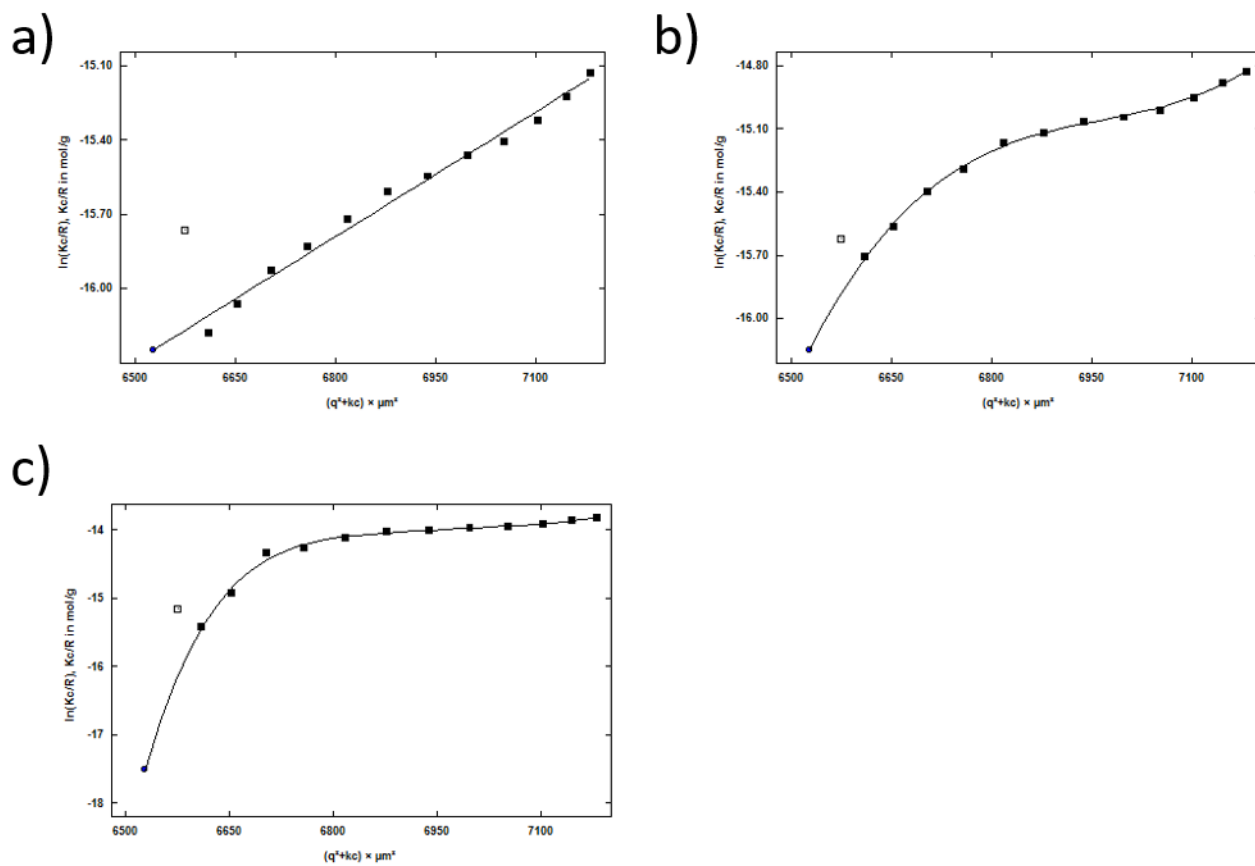


Figure S14. SLS studies of aggregated species **1** (a) **2A** (b) and **2B** (c) and corresponding Guinier Plot. All studies have been performed at 298 K with the corresponding aggregate solutions (20 μ M, 10% (**1** and **2A**) or 35% THF (**2B**)).

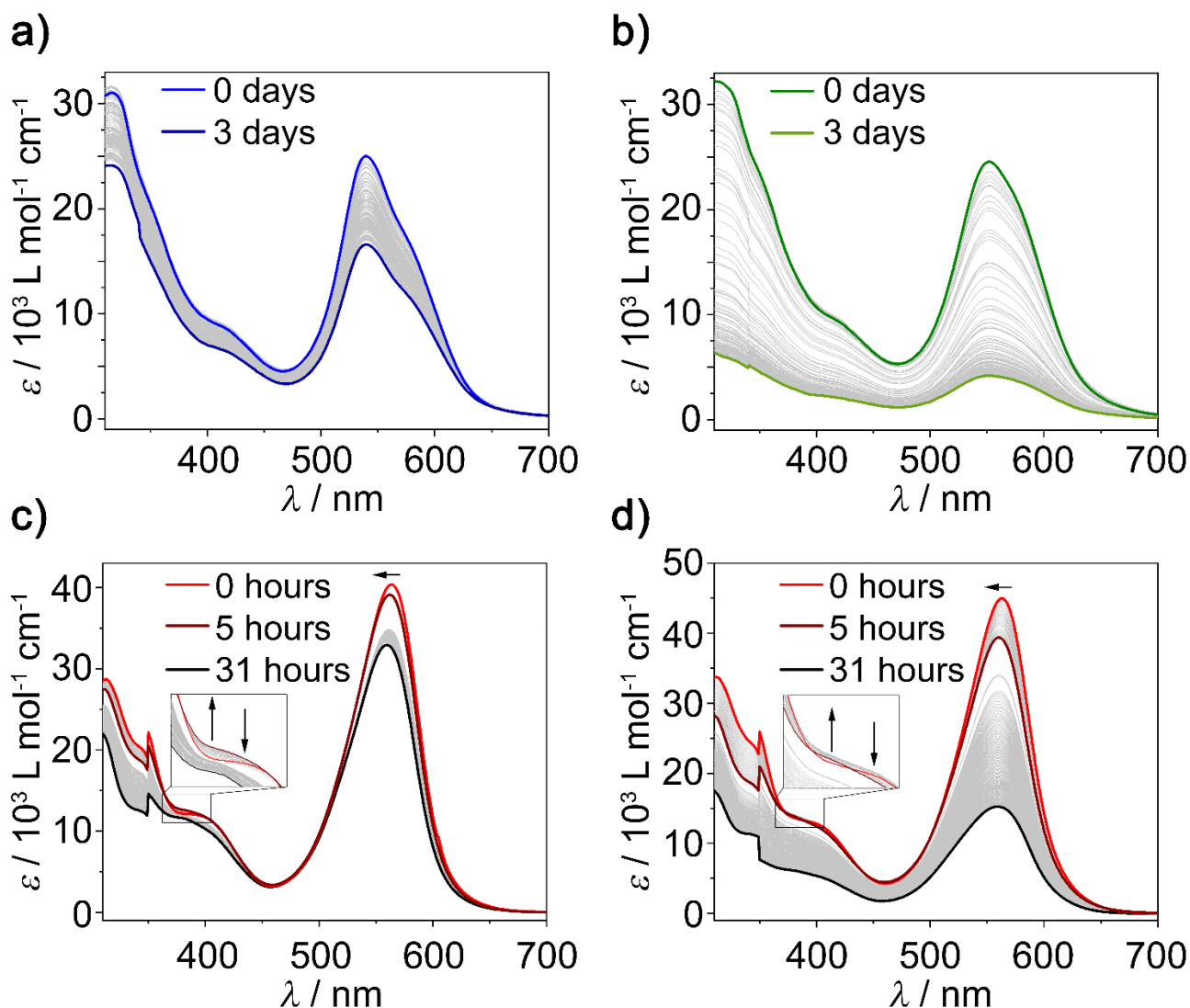


Figure S15. Time-dependent UV-Vis spectra at acidic conditions (pH = 4) for **1** (a,c) and **2** (b,d) with different amounts of THF: 10% (a,b) and 50% (c,d) at $c = 20 \mu\text{M}$ and 298 K.

The hydrazone bond, which is connecting the hydrophobic residue with the BODIPY dye, is known to be responsive and cleavable by hydrolysis under acidic conditions. The responsive behavior of this bond was investigated by changing the dynamics of the systems (co-solvent ratio was alternated) at pH 4 and accordingly the corresponding absorption changes were recorded over time (Figure S15).

Overall, it has been found that the aggregates tend to precipitate under acidic conditions. This most likely occurs due to the intercalation of charged solvent molecules, which may destabilize the hydration shell formed by the TEG chains. However, despite the decrease of absorption, no significant changes in the absorption signature of aggregates of **1** and **2** has been found over time at low THF content (10%) and pH 4 (Figure S15a-b). With increasing THF content (20%), the absorption signatures change for **1**, while the spectral shifts remain the same for **2** (Figure S16). This can be explained with help of the denaturation curves (Figure 1b and d), which reinforces the higher stability of **2** and therefore also lower dynamics are observed for this aggregate. Due to the lower dynamics, less water can penetrate into the hydrophobic interior and react with the hydrazone bond to yield the free aldehyde. With increasing amounts of THF (30 or 40%), more drastic absorption changes are also found for **2**, suggesting the cleavage of this hydrazone bond (Figure S16). If **1** and **2** are investigated at 50% THF, where both exist in a monomeric state, a minor blue-shift with simultaneous increase of a characteristic band at 380 nm is observed after 5 hours (Figure S15 and S16e). This band has been recently assigned to the functionalization of a conjugated aldehyde group and therefore underlines the hydrolysis to free aldehyde (Figure S8e).³ Also, the minor red-shift of the monomeric BODIPY band agrees with the formation of the BODIPY compound with free aldehyde (Figure S8e).³

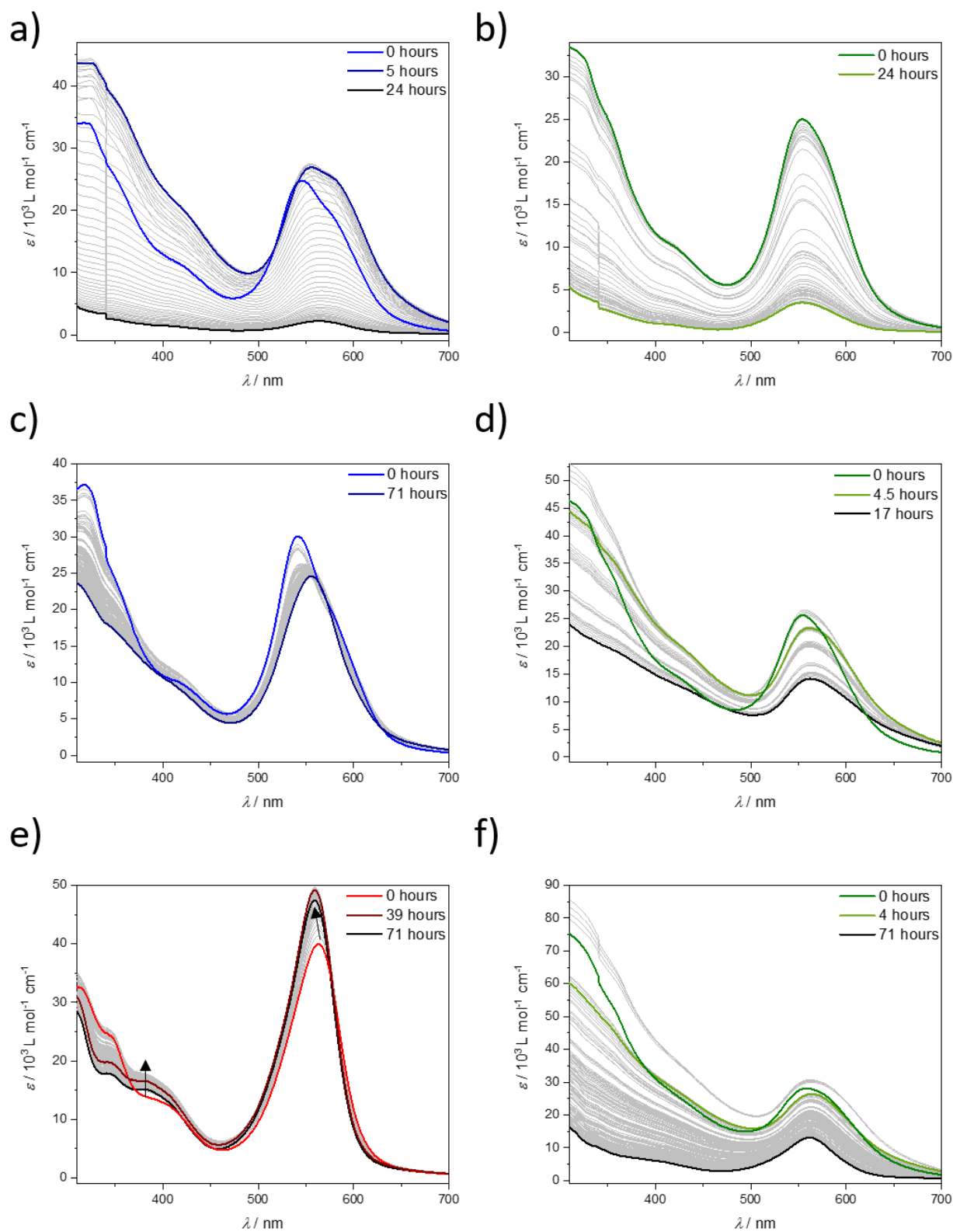


Figure S16. Time-dependent UV-Vis studies of **1** (a, c, e) and **2** (b, d, f) at different water/THF ratios: 2/8 (a-b), 3/7 (c-d), 4/6 (e-f, v/v) at acidic conditions pH = 4, 298 K and $c = 20 \mu\text{M}$.

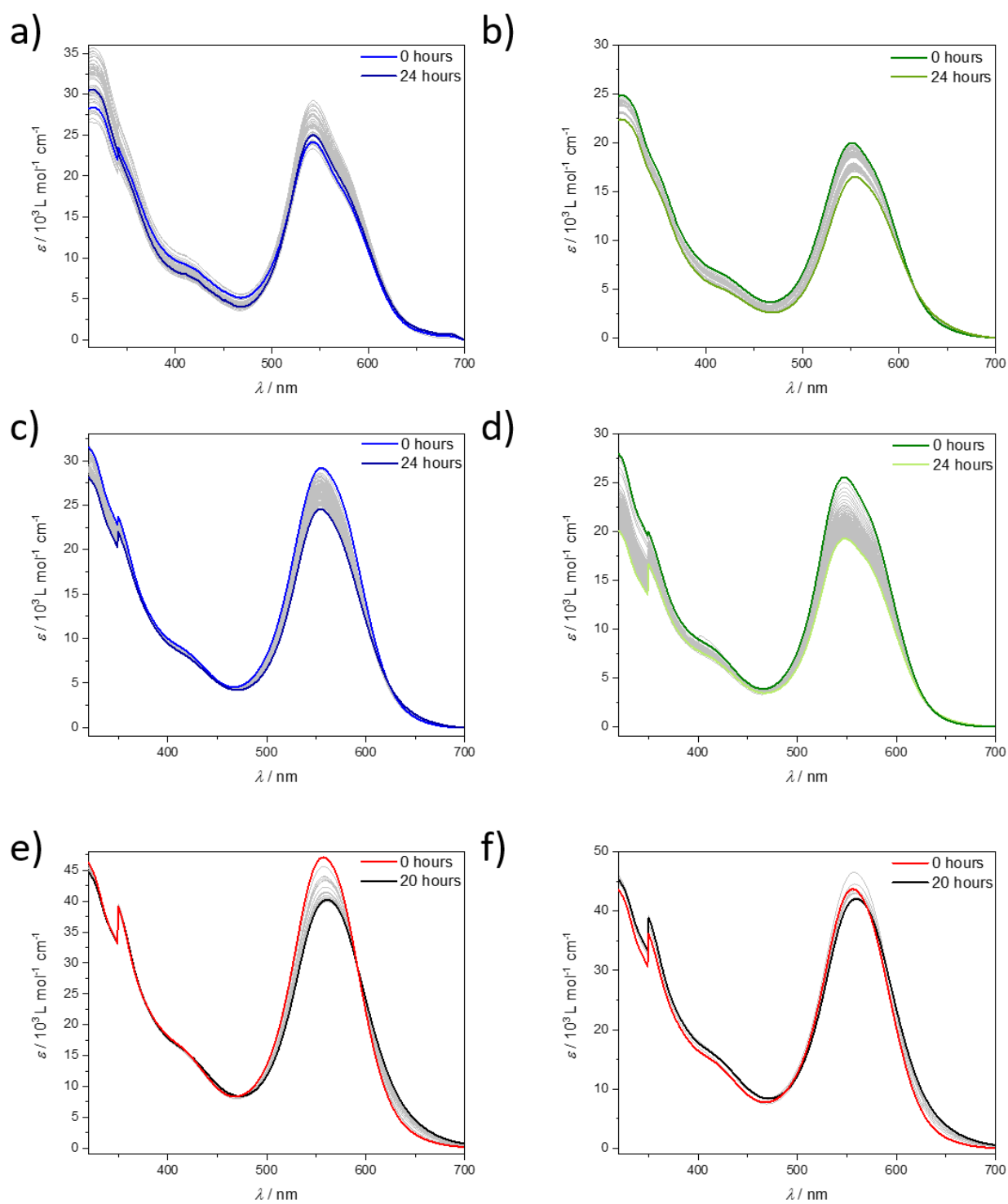


Figure S17. Time-dependent UV-Vis studies of **1** (a, c, e) and **2** (b, d, f) at different water/THF ratios: 2/8 (a-b), 3/7 (c-d), 4/6 (e-f, v/v) at neutral conditions pH = 7, 333 K and $c = 20 \mu\text{M}$.

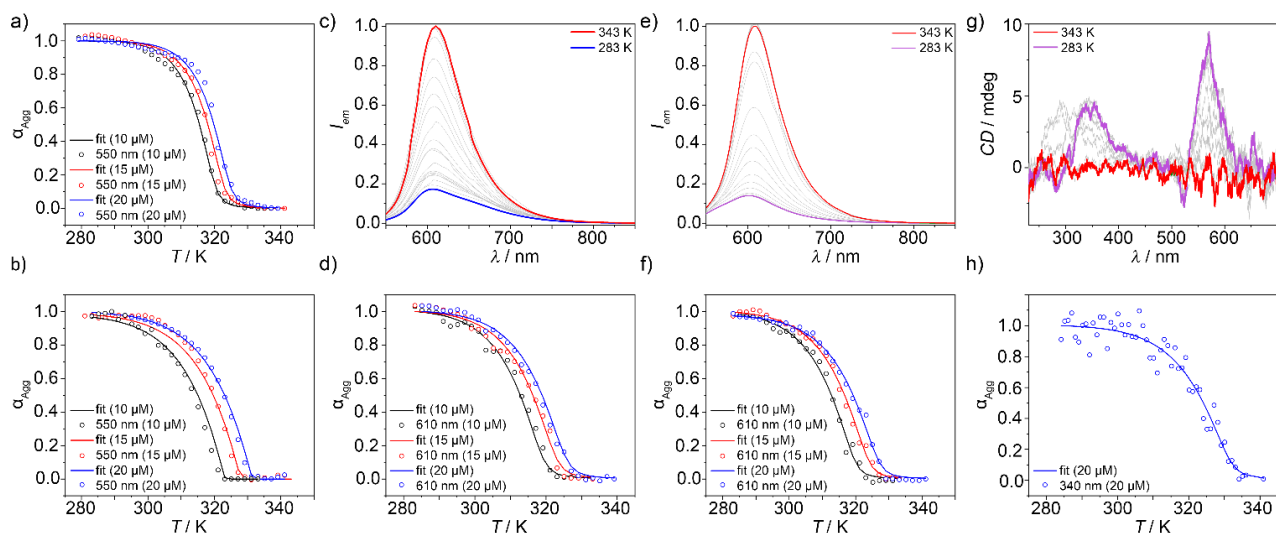


Figure S18. Plot of α_{agg} vs. Temperature extracted from VT UV-Vis at $\lambda = 550$ nm (a,b), VT emission studies at 610 nm (d,f) or VT CD studies at 340 nm and corresponding fits to the nucleation-elongation model for **1** (a,d) and **2B** (b,f,h). VT emission (c,e) and CD (g) spectra of **1** (25/75, THF/H₂O (v/v)) and **2B** (35/65, THF/H₂O (v/v)) at 20 μ M between 343 K and 283 K. $\lambda_{exc} = 530$ nm was used for emission studies.

We also performed additional variable temperature (VT)-spectroscopy studies (UV-Vis, emission and CD) as a tool to investigate the mechanistic pathways of **1** and **2**. However, to ensure that no cleavage of the hydrophobic residue will occur during these experiments, we used fast cooling ramps (2K min⁻¹, Figure S18-21).

To reach the monomer at 333 K ($c = 10$ -20 μ M), the addition of 25% for **1** and 35% of THF for **2** was needed. The VT-absorption studies show the inverse spectroscopic behavior upon cooling as previously observed by denaturation studies: Decrease of the monomeric band with the emergence of the blue-shifted aggregate band (Figure S19). Global fitting^{4,5} of the observed degree of aggregation vs. T yields the thermodynamic parameters for these systems at a specific THF content ($\Delta G = -37.4$ kJmol⁻¹ (**1**), $\Delta G = -34.3$ kJmol⁻¹ (**2B**), Figure S18a-b, Table S2). In comparison to previous denaturation studies, the Gibbs energy is higher (lower negative values), which is not surprising as the addition of THF during these VT-studies weakens the overall aggregation tendency.¹⁰

Since the THF content for the VT-experiments of **2B** (35% THF) is higher than for **1** (25% THF), these differences in the solvent mixture rationalize the higher Gibbs energy for **1** in comparison to **2B**. Therefore, denaturation studies are more accurate for comparison of **1** and **2**, as they cover the complete disassembly process via addition of a good solvent (THF) and not the stability of the aggregates at a specific single THF content.

The VT-emission studies exhibit the quenching of emission upon cooling, which furthermore supports that **1** and **2B** self-assemble in a face-to-face fashion (Figure S18c,e, S20). Mathematical analysis by global fitting^{4,5} of the experimental data unveils thermodynamic parameters that are in agreement with absorption studies (Figure S18d,f and Table S2).

VT-CD studies also support the two-step transition of **2** upon disassembly, which has been observed during denaturation studies. However, we were unable to obtain a complete **M** \rightarrow **2B** \rightarrow **2A** transition, possibly due to the high sensitivity of the aggregate stability to changes in solvent composition (Figure S18g,h and S21). With the same THF content as recently used for the VT-absorption and emission studies, the increase of the positive CD signals at 340 and 550 nm is observed (**M** \rightarrow **2B**, Figure S18g,h and S21). Plotting the CD changes at 340 nm also yields a cooperative curve with comparable thermodynamic parameters to emission and absorption studies (Figure S18h, S21 and Table S2). However, due to the high signal to noise ratio these studies have to be treated with care and should only give a rough estimation of the thermodynamic parameters. Note, that with decreased concentrations the signal to noise ratio worsens, hence different concentrations have not been globally fitted.

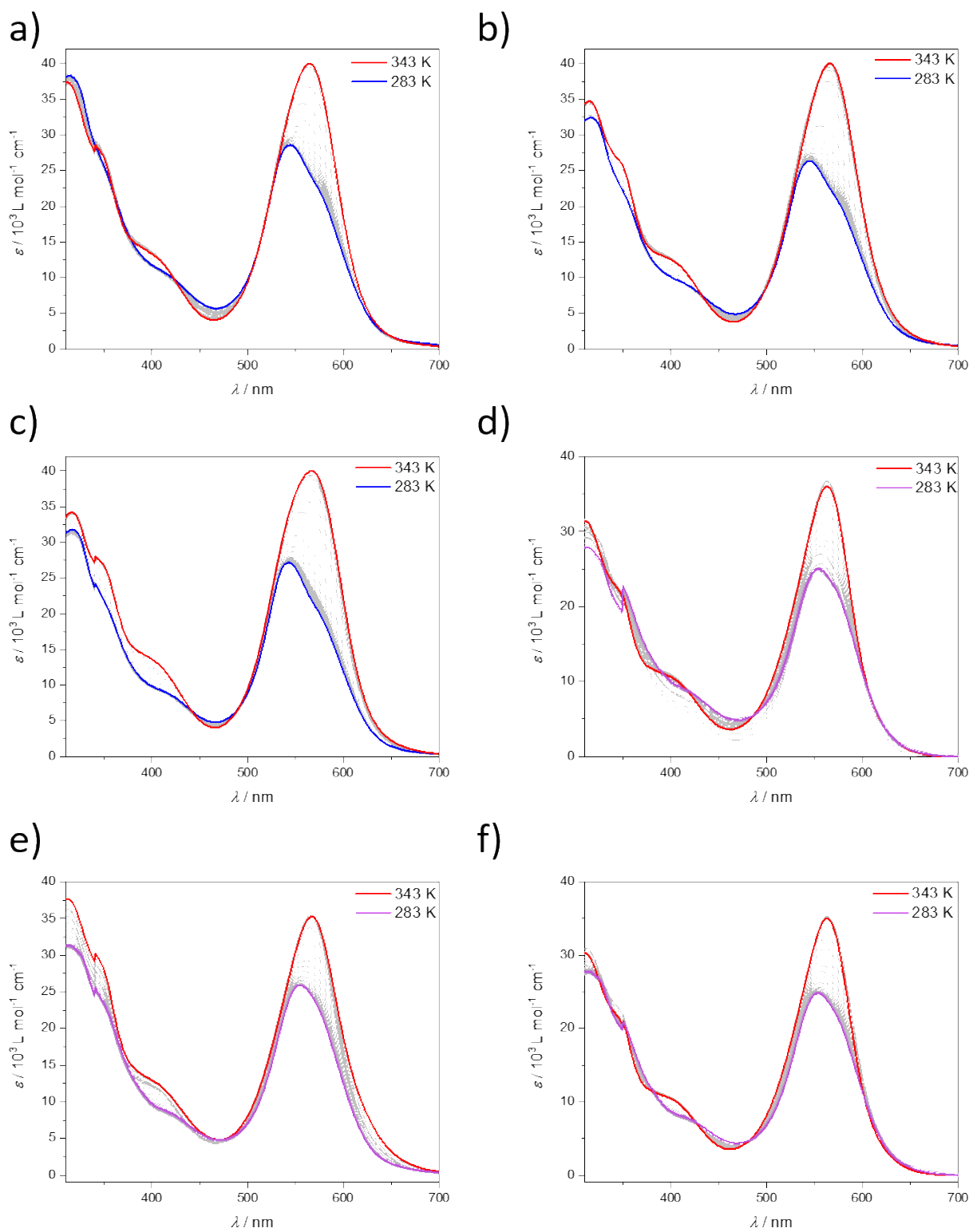


Figure S19. VT UV-Vis spectra of **1** (water/THF 75/25 (v/v), a-c) and **2** (water/THF 65/35 (v/v), d-f) with fast cooling: 2 Kmin⁻¹ from 343-283 K at multiple concentrations: $c = 10$ (a,d), 15 (b,e), 20 μM (c,f).

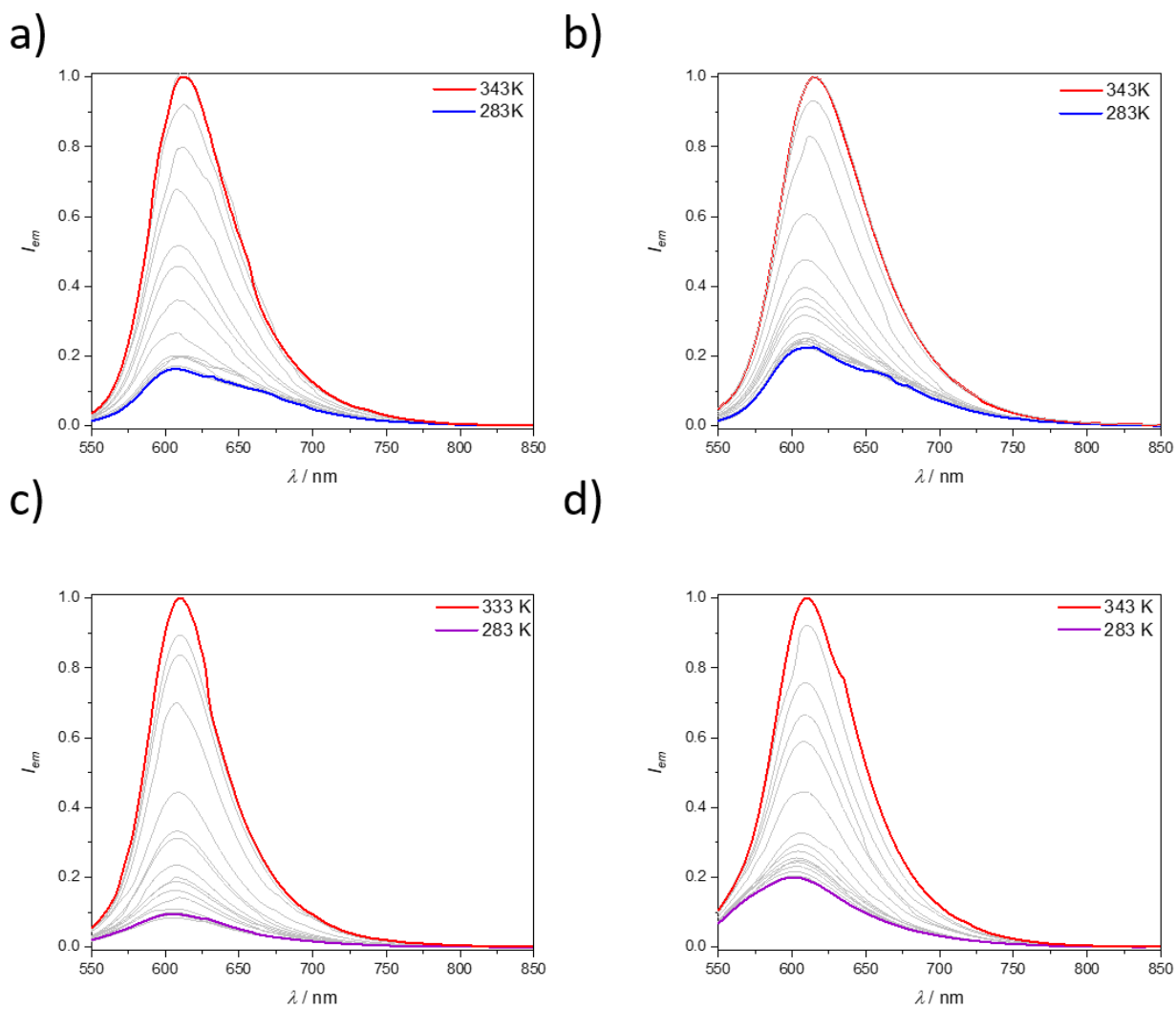


Figure S20. VT Emission spectra of **1** (water/THF 75/25 (v/v), a-b) and **2** (water/THF 65/35 (v/v), c-d) with fast cooling: 2 Kmin^{-1} from 343-283 K at multiple concentrations: $c = 10$ (a,c), $15 \mu\text{M}$ (b,d).

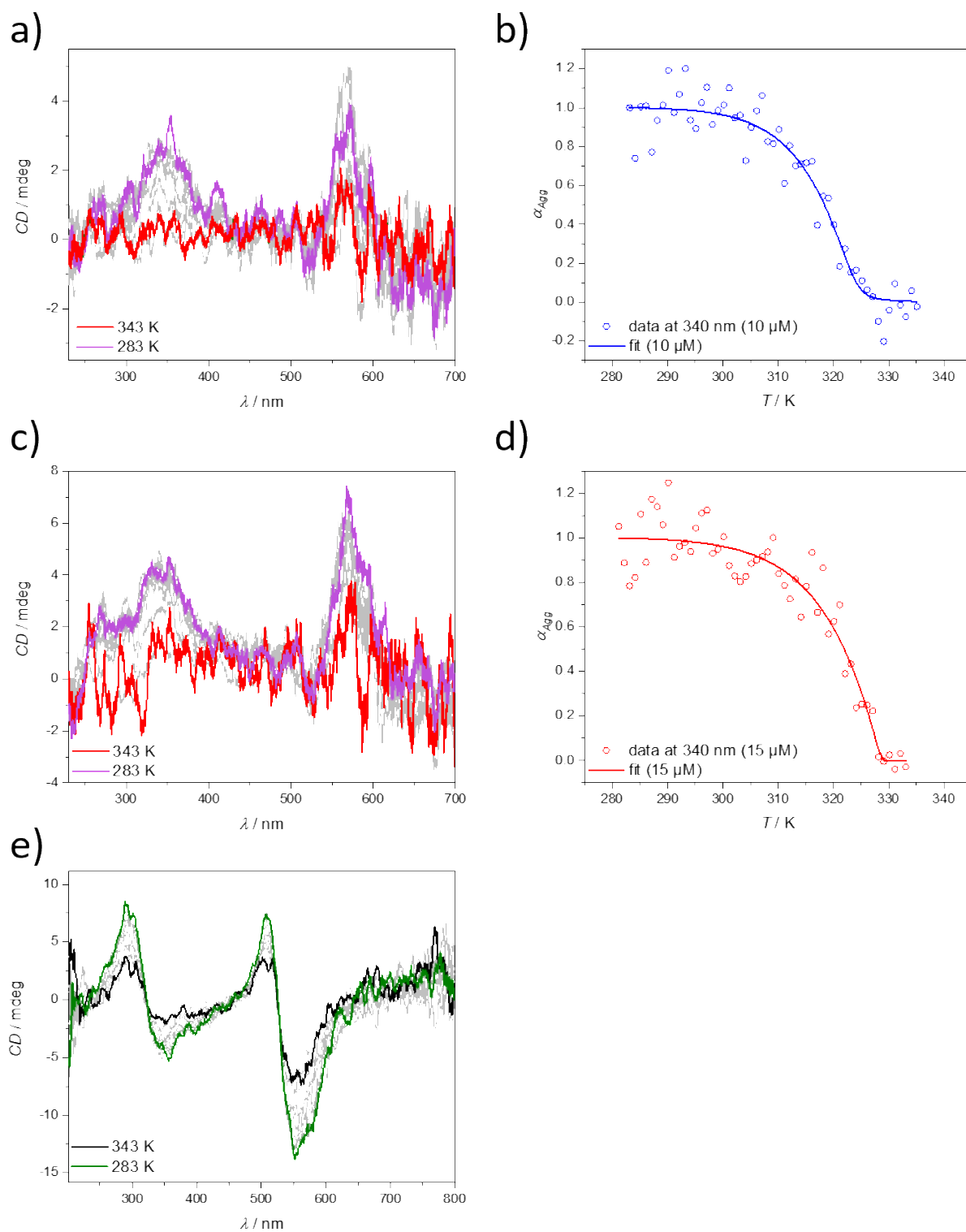


Figure S21. VT CD spectra (a,b) and CD changes (c,d) at 340 nm of **2** (water/THF 65/35 (v/v), a-d) with fast cooling: 2 Kmin⁻¹ from 343-283 K at multiple concentrations: $c = 10$ (a,c), 15 μ M (b,d). e) VT CD spectra of **2** (water/THF 85/15 (v/v) with fast cooling: 2 Kmin⁻¹ from 343-283 K at $c = 20$ μ M.

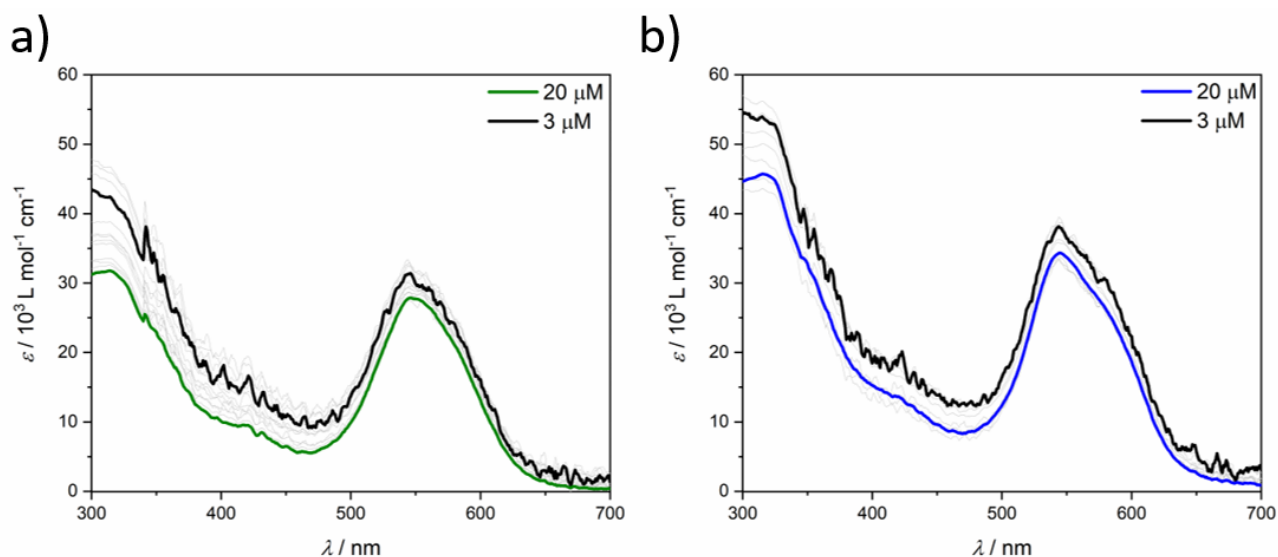


Figure S22. UV-Vis spectra of **1** (a) and **2** (b) at room temperature and concentrations ranging from 20 to 3 μM in water (traces of THF might be present after removal of the residual co-solvent (1% THF)).

No spectral changes are found at the lowest possible concentration (UV-Vis absorption was under 0.05), which highlights the high stability of the assemblies formed by both amphiphiles and the importance of entropic interactions to stabilize them.

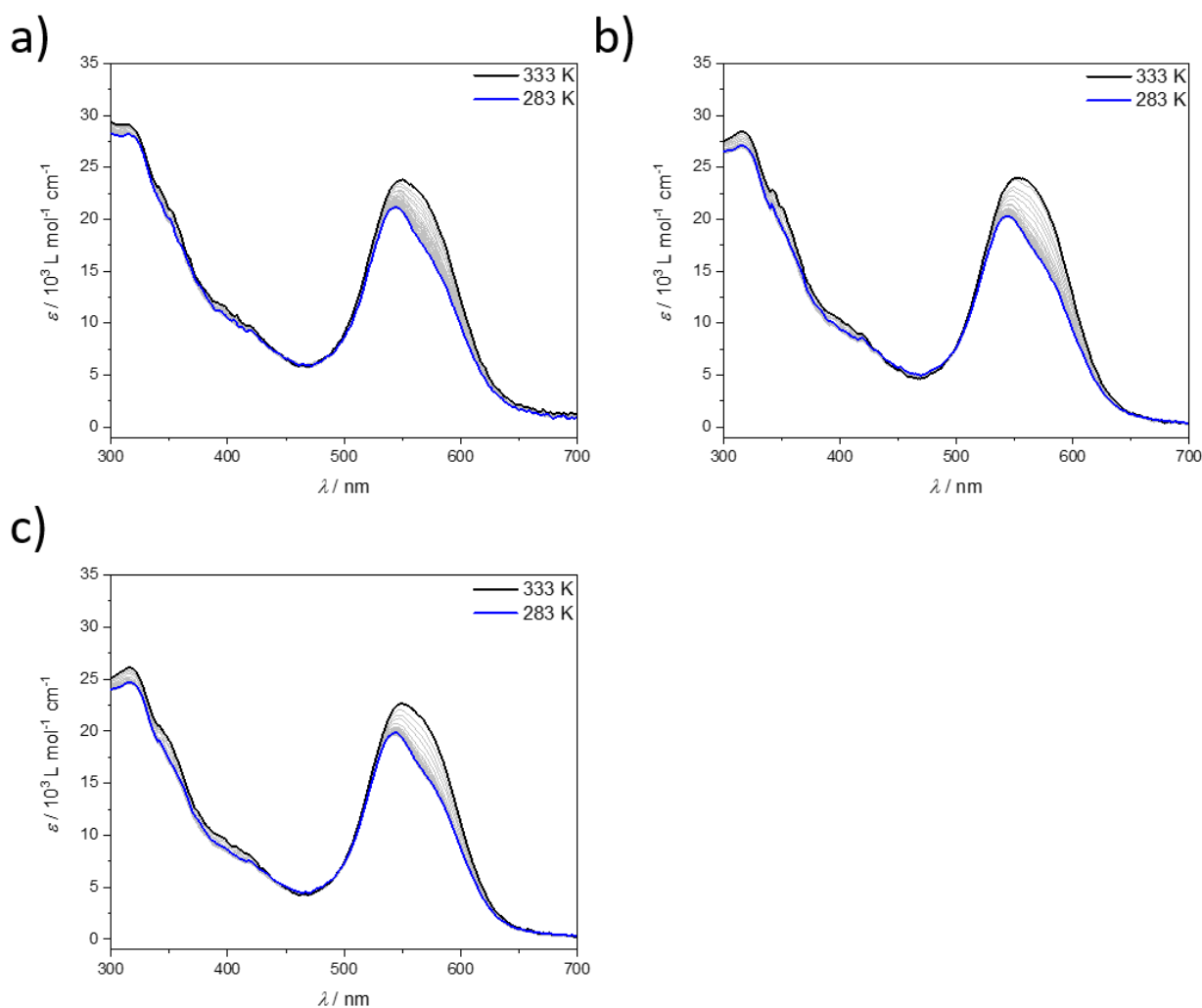


Figure S23. VT UV-Vis spectra of **1** (water/THF 85/15 (v/v), a-c) with fast cooling: 2 Kmin^{-1} from 343-283 K at multiple concentrations: $c = 10$ (a,d), 15 (b,e), 20 μM (c,f).

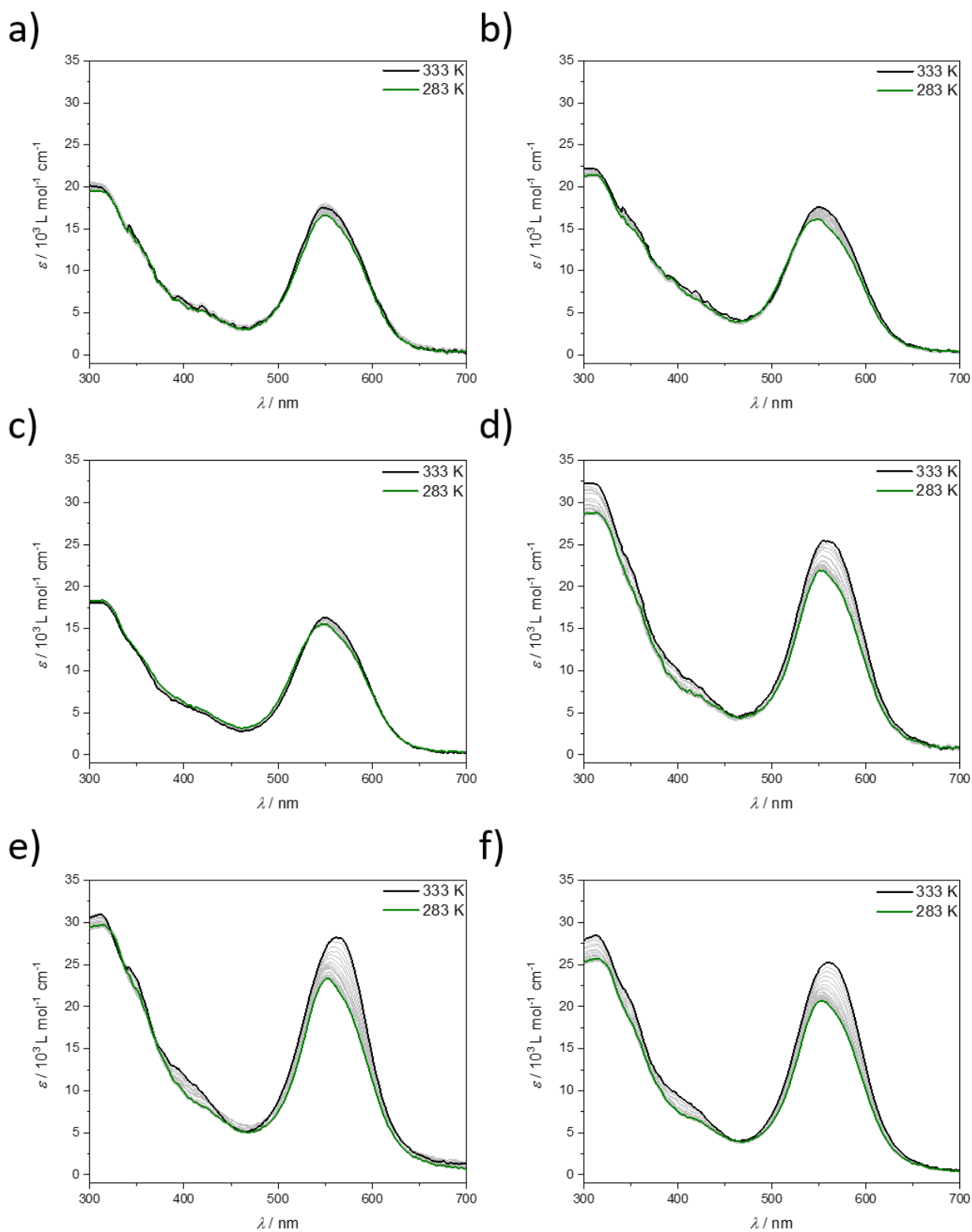


Figure S24. VT UV-Vis spectra of **2** (water/THF 85/15 (v/v, a-c) and 75/25 (v/v, a-c)) with fast cooling: 2 Kmin⁻¹ from 343-283 K at multiple concentrations: *c* = 10 (a,d), 15 (b,e), 20 μM (c,f).

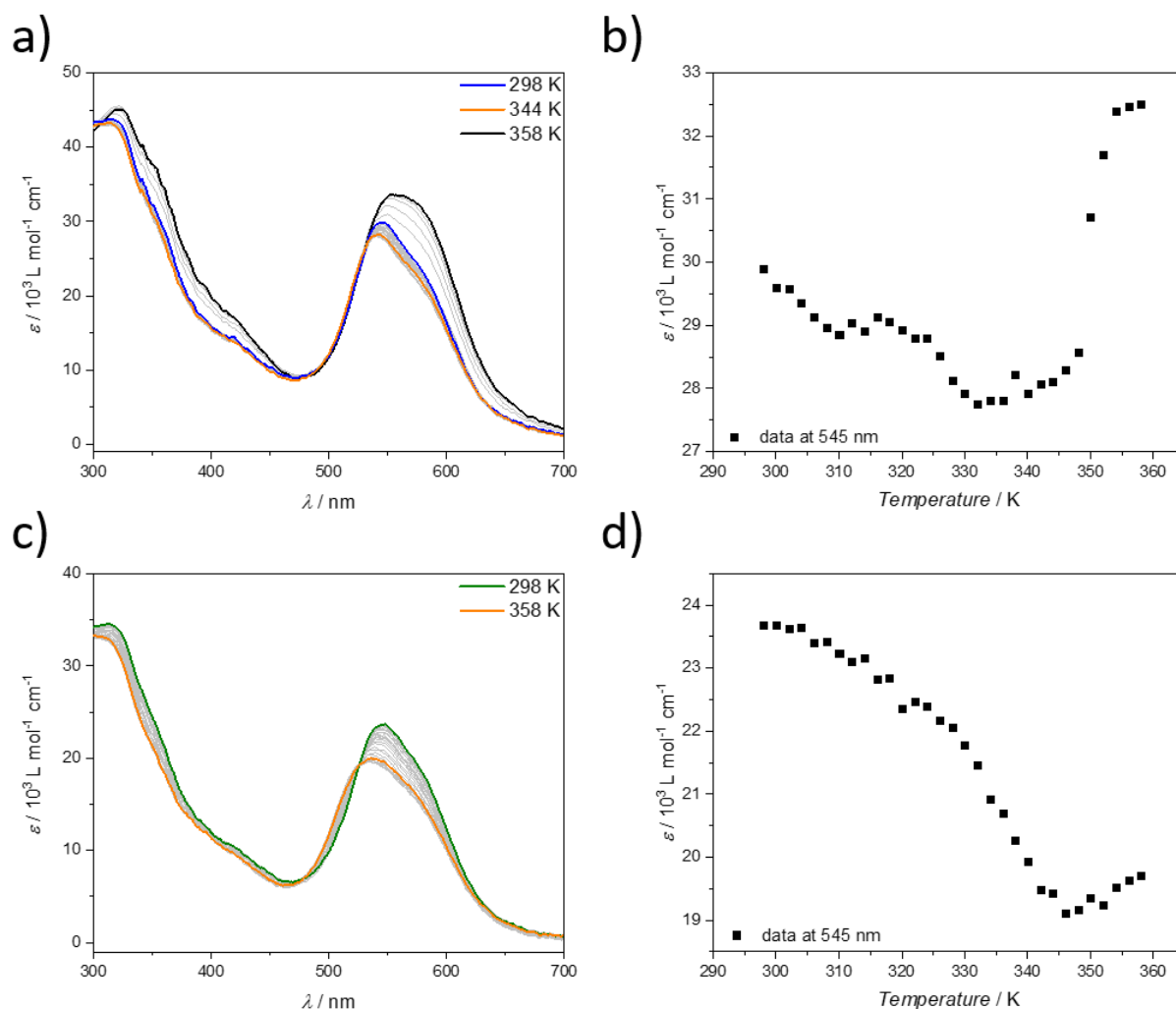


Figure S25. VT UV-Vis spectra (a,c) and plot of ϵ vs. temperature (b,d, extracted from VT UV-Vis at $\lambda = 545 \text{ nm}$) for **1** (a,b) and **2** (c-d) with fast heating: 2 Kmin^{-1} from 298-358 K in water (traces of THF might be present after removal of the residual co-solvent (1% THF)) at $c = 20 \mu\text{M}$.

Heating the assembly of **1** and **2** in pure water leads to a blue-shift and decrease of the molar extinction coefficient (orange plot in Fig S25a or c). This can be rationalized by the partial dehydration of the TEG chains at high temperatures (please see critical temperature in Fig S25b for **1**: 332 K and Fig S25c for **2**: 346 K), which is influencing the packing of **1** and **2**. Even more, a second process is observed for **1** starting at 340 K and can be referred to the partial disassembly of the self-assembled structure (Fig S25a,b).

References

- 1 K.-H. Yin, Y.-H. Hsieh, R. S. Sulake, S.-P. Wang, J.-I. Chao, C. Chen, *Bioorg. Med. Chem. Lett.* **2014**, *24*, 5247.
- 2 M. Kanamala, B. D. Palmer, H. ghandehari, W. R. Wilson, Z. Wu, *Pharm. Res.* **2018**, *35*,154.
- 3 I. Helmers, M. Niehues, K. K. Kartha, B. J. Ravoo, G. Fernández, *Chem. Commun.* **2020**, *56*, 8944.
- 4 H. M. M. Ten Eikelder, A. J. Markwoort, T. F. A. De Greef, P. A. J. Hilbers, *J. Phys. Chem. B* **2012**, *116*, 5291-5301
- 5 A. J. Maarkvort, H. M. M. Ten Eikelder, P. J. J. Hilbers, T. F. A. De Greef, E. W. Meijer, *Nat. Commun.* **2011**, *2*, 509-517.
- 6 P. A. Korevaar, C. Schaefer, T. F. A. de Greef, E. W. Meijer, *J. Am. Chem. Soc.*, **2012**, *134* (32), 13482–13491.
- 7 Goldstein, R. F.; Stryer, L. *Biophys. J.*, **1986**, *50*, 583-599.
- 8 J. Israelachvili, *Intermolecular and Surface Forces*, 2nd ed., Academic Press, San Diego, 1991.
- 9 L. Yang, G. Fan, X. Ren, L. Zhao, J. Wang, Z. Chen, *Phys. Chem. Chem. Phys.* **2015**, *17*, 9167.
- 10 D. Görl, F. Würthner, *Angew. Chem. Int. Ed.* **2016**, *55*, 12094.